nature geoscience

ARTICLES

https://doi.org/10.1038/s41561-019-0502-8

Importance of wind and meltwater for observed chemical and physical changes in the Southern Ocean

Ben Bronselaer[1,2,3]*, Joellen L. Russell[1], Michael Winton[2], Nancy L. Williams[4], Robert M. Key[3], John P. Dunne[2], Richard A. Feely[5], Kenneth S. Johnson[6] and Jorge L. Sarmiento[3]

The Southern Ocean south of 30° S represents only one-third of the total ocean area, yet absorbs half of the total ocean anthropogenic carbon and over two-thirds of ocean anthropogenic heat. In the past, the Southern Ocean has also been one of the most sparsely measured regions of the global ocean. Here we use pre-2005 ocean shipboard measurements alongside novel observations from autonomous floats with biogeochemical sensors to calculate changes in Southern Ocean temperature, salinity, pH and concentrations of nitrate, dissolved inorganic carbon and oxygen over two decades. We find local warming of over 3 °C, salinification of over 0.2 psu near the Antarctic coast, and isopycnals are found to deepen between 65° and 40° S. We find deoxygenation along the Antarctic coast, but reduced deoxygenation and nitrate concentrations where isopycnals deepen farther north. The forced response of the Earth system model ESM2M does not reproduce the observed patterns. Accounting for meltwater and poleward-intensifying winds in ESM2M improves reproduction of the observed large-scale changes, demonstrating the importance of recent changes in wind and meltwater. Future Southern Ocean biogeochemical changes are likely to be influenced by the relative strength of meltwater input and poleward-intensifying winds. The combined effect could lead to increased Southern Ocean deoxygenation and nutrient accumulation, starving the global ocean of nutrients sooner than otherwise expected.

In the Southern Ocean, strong westerly winds drive vertical mixing between surface and deep waters[1,2]. In the early 2000s, Southern Ocean temperature and salinity changes were largely passive, driven by atmospheric fluxes, and subject to little dynamic influence[3–5]. An increase and poleward shift in these westerly winds has been inferred from reanalyses since 1980[6,7], yet models from the Phase 5 of the Coupled Model Intercomparison Project (CMIP5) underestimate these historical trends[6].

The CMIP5 models also fail to appropriately account for Antarctic ice sheet meltwater[8], which has accelerated over the past few decades[9,10], and which has been shown to significantly affect climate projections[8]. Both winds and meltwater affect ocean ventilation south of the Antarctic Circumpolar Current (ACC), where surface waters are mixed with deep Antarctic bottom water. This ventilation leads to the upwelling of warm water rich in carbon, with the potential to influence sea ice, atmospheric temperature and CO_2 levels[1,11–15]. North of the ACC, winds affect intermediate and mode water formation, which feeds the world's ocean with nutrients[1,16] and stores anthropogenic carbon and heat[4,17,18]. Poleward-intensifying winds increase mixing, thereby strengthening deep water ventilation and mode water formation[19–21], while meltwater freshens the surface ocean and reduces vertical mixing.

We use state-of-the-art measurements from biogeochemical floats from the Southern Ocean Carbon and Climate Observations and Modeling (SOCCOM) project, spanning the years 2014–2019 (up to March 2019) and shipboard data collected before 2005 (centred roughly around the year 1995) to identify recent changes in Southern Ocean temperature, salinity, nitrate, dissolved inorganic carbon (DIC), oxygen and pH. We find significant warming, salinification and deoxygenation around the Antarctic coast outside the range of simulated natural variability. Isopycnals are found to deepen north of 65° S, where ocean deoxygenation, acidification and carbon uptake are reduced.

We use a five-member ensemble of a historical–representative concentration pathway (RCP) 8.5 climate change projection with the Geophysical Fluid Dynamics Laboratory (GFDL) Earth system model ESM2M (referred to as the standard scenario or SS, see Methods), subsampled on the same grid as the observations, to demonstrate that ESM2M does not capture the observed patterns of change in the Southern Ocean. We propose that Antarctic meltwater and poleward-intensifying westerly winds are important forcing agents that influence the contemporary Southern Ocean's response to climate change. Accounting for these forcing agents can improve reproduction of observed physical and biogeochemical changes. To demonstrate the importance of poleward-intensifying wind and ice sheet meltwater, we apply step perturbations: a 0.02 Sv idealized meltwater flux around Antarctica, as well as a 10% intensification and 0.4° poleward shift of the Southern Ocean westerlies to the same ensemble members of the RCP 8.5 ESM2M experiments starting in the year 2005 (referred to as the wind–meltwater scenario, WMS). These perturbations are comparable in magnitude to inferred observed changes (Methods). We also apply the same wind and meltwater perturbations separately to the same five ensemble members to attribute simulated anomalies, referred to as the

[1]Department of Geosciences, University of Arizona, Tucson, AR, USA. [2]Geophysical Fluid Dynamics Laboratory (NOAA), Princeton University Forrestal Campus, Princeton, NJ, USA. [3]Program in Atmospheric and Oceanic Sciences, Princeton University, Princeton, NJ, USA. [4]College of Marine Science, University of South Florida, Saint Petersburg, FL, USA. [5]Pacific Marine Environmental Laboratory (NOAA), Seattle, WA, USA. [6]Monterey Bay Aquarium Research Institute, Moss Landing, CA, USA. *e-mail: bbronselaer@email.arizona.edu

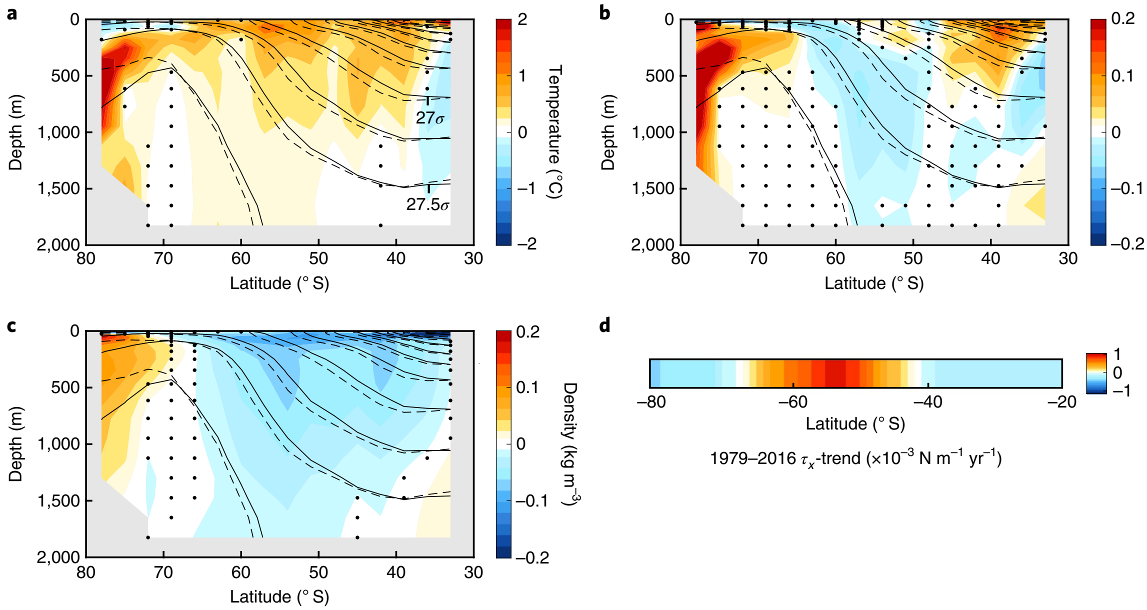

Fig. 1 | Observed physical changes. a–c, Zonal mean differences in temperature (**a**), salinity (**b**) and potential density (**c**, referenced to 0 m depth) between 2014 and 2019 SOCCOM data and pre-2005 shipboard data. The comparison is only shown where there is overlap between both datasets on an 8°x 3° horizontal grid. Solid and dashed lines show zonal mean shipboard and SOCCOM isopycnal surfaces, respectively. Grey shading denotes areas with insufficient data. The stippling indicates where the differences are not significant at the 90% level, and includes both observational uncertainty as well as natural variability (see Methods). Areas that are not stippled are therefore directly forced by climate change. **d**, The linear trend in Southern Ocean zonal wind stress between 1979 and 2016, as calculated from the mean of the ERA-interim and the NCEP-DOE AMIP-II reanalyses[43,44], shown at the same latitudes as **a**–**c**.

wind-only and meltwater-only scenarios, respectively. We also perform a 5 × WMS ensemble of five members with larger perturbations of 0.1 Sv and 50% wind intensification to demonstrate that our conclusions do not depend on the exact magnitude of the forcing, and explore the potential future impact of wind and meltwater. The large-scale patterns of change are poorly represented in our climate model, which simulates mostly passive changes driven by atmospheric fluxes, but increasing Southern Ocean wind and meltwater forcing improves the simulations and affects future biogeochemical properties, thereby demonstrating the influence of these forcings.

Observed decadal changes

The SOCCOM floats provide novel insight by sampling year-round, under-ice and biogeochemical data across the Southern Ocean. Figure 1 shows the changes in temperature, salinity and potential density between the SOCCOM dataset and pre-2005 shipboard data, and corresponding changes in isopycnal surfaces. Figure 1 is complemented by the same comparison including all of the Argo[22] data from 2014–2019 in Extended Data Fig. 1. As both SOCCOM and shipboard data provide partial coverage of the Southern Ocean, we calculate only decadal changes where there is overlap between the two datasets (Extended Data Fig. 2). SOCCOM coverage is better to the south than to the north of 40° S, so anomalies shown north of 40° S are less representative of the zonal mean. However, the temperature and salinity are consistent with the larger spatial coverage when including the full Argo dataset (see Methods). Most Southern Ocean shipboard measurements are taken between December and May, so we use to the SOCCOM year-round coverage to effectively remove the effect of seasonal bias from the comparison (see Extended Data Fig. 9).

Isopycnals are observed to shallow south of 65° S, where salinity increased by up to 0.2 psu. This increase in salinity coincides with a mean subsurface warming of up to 3 °C at 400 m depth. South of 65° S, the salinification and warming have opposing effects on the density, with the salinity effect being dominant. The observed warming around the Antarctic coast is located in the Ross and Amundsen seas, as well as along the Amery Ice shelf and south of Tasmania (Extended Data Fig. 2). Between 65° S and 40° S, the Southern Ocean is warming[23] and becoming fresher, coinciding with a stronger deepening of the isopycnals than previously observed[3].

Figure 2 shows decadal changes in oxygen, DIC and nitrate concentrations and pH. Data coverage varies across the sampled biogeochemical variables, with ample oxygen, temperature and salinity sampling south of 65° S, but fewer data for DIC and nitrate concentrations and pH. South of 65° S, significant decreases in oxygen and pH are observed around the Antarctic coast, while nitrate and DIC concentrations are increasing. Close to the coast, subsurface oxygen concentrations have decreased by 60 μmol kg^{-1}, while pH has decreased by over 0.13. While large-scale deoxygenation is consistent with earlier studies[24], the deoxygenation near the Antarctic coast is larger than previously observed. The pH anomaly is negatively correlated with the DIC and nitrate anomalies and positively correlated with the oxygen anomaly (with correlation coefficients of −0.75, −0.39 and 0.32, respectively). The relationship with DIC is strongest, suggesting that pH changes are mostly due to anthropogenic acidification (see Methods), and showing a distinct anthropogenic influence throughout the Southern Ocean, contrary to previous studies[4].

Overall, observations show significant isopycnal shallowing outh of 65° S. Between 65° S and 40° S, where isopycnals deepen, changes are generally not statistically significant below 500 m depth. This pattern is consistent with decadal changes between the 2000–2013 and pre-2000 Global Ocean Data Analysis Project version 2 (GLODAPv2) synthesis products[25] (Supplementary Fig. 1). A decomposition of observed DIC changes into anthropogenic and dynamical changes (Extended Data Fig. 3) shows that dynamical changes cause a reduction in DIC in the region of isopycnal deepening.

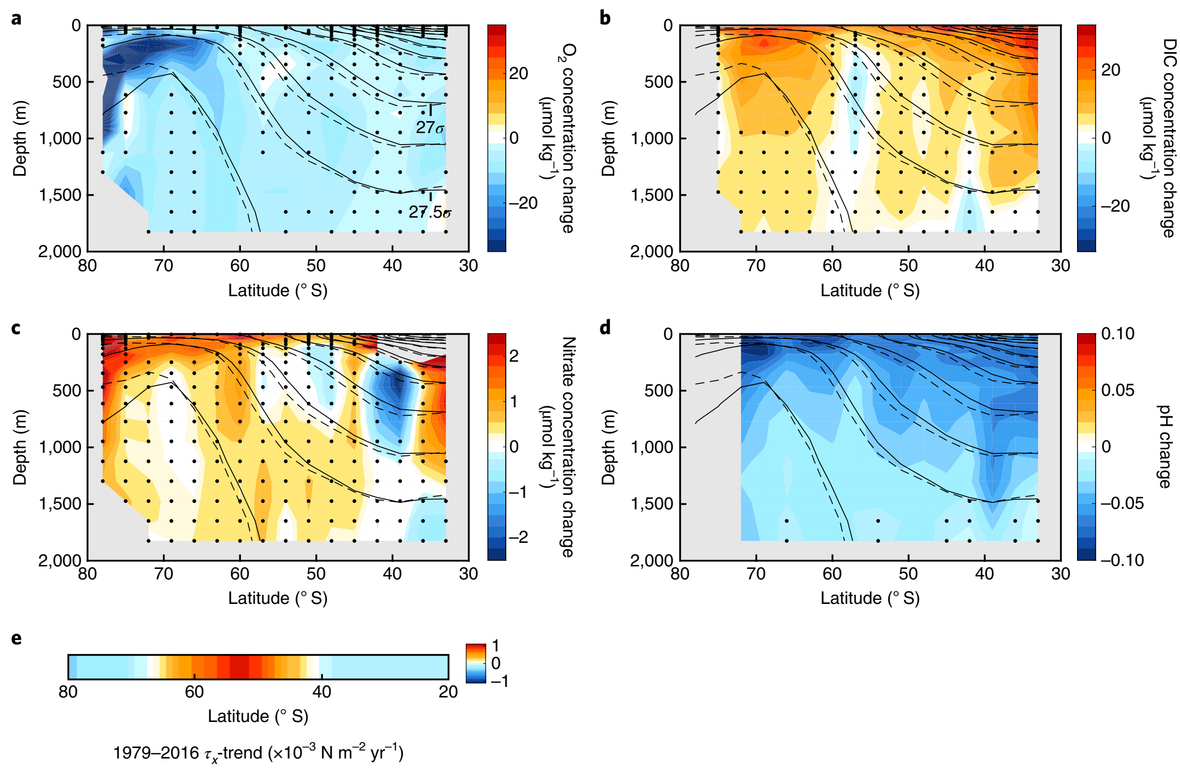

Fig. 2 | Observed biogeochemical changes. a–d, Zonal mean differences in oxygen (**a**), DIC (**b**) nitrate (**c**) concentrations and pH (**d**) between 2014 and 2019 SOCCOM data and pre-2005 shipboard data. The comparison is only shown where there is overlap between both datasets on an 8° × 3° horizontal grid. Solid and dashed lines show zonal mean shipboard and SOCCOM isopycnal surfaces, respectively. Grey shading denotes areas with insufficient data. The stippling indicates where the differences are not significant at the 90% level, and includes both observational uncertainty as well as natural variability (see Methods). Areas that are not stippled are therefore directly forced by climate change. **e**, The linear trend in Southern Ocean zonal wind stress between 1979 and 2016, as calculated from the mean of the ERA-interim and the NCEP-DOE AMIP-II reanalyses[43,44], shown at the same latitudes as **a**–**d**.

We find more data overlap between SOCCOM and shipboard data nearer Drake Passage, with sparser overlap elsewhere (Extended Data Fig. 2). The zonal means shown in Figs. 1 and 2 are therefore biased towards the region around Drake Passage[26]. The observed subsurface warming and increase in salinity South of 60° S is strongest in the Pacific Ocean sector, and the Indian and Pacific sectors show increases in oxygen North of 60° S (Supplementary Figs. 2–4).

Simulated wind–meltwater influence

We use the ESM2M SS to better understand the observed physical and biogeochemical anomalies. We find that simulated temperature and salinity changes in the SS are weaker and shallower than observed, such that the simulated isopycnal deepening is not significant below 500 m depth (Fig. 3). The model does not simulate significant coastal warming and salinification near the Antarctic coast. The simulated nitrate changes are negatively correlated with observations. The model simulates a large-scale increase in DIC, but weaker dynamic DIC changes compared with observations (see Extended Data Fig. 3).

Figure 4 shows the same decadal changes as Fig. 3 for the WMS, subsampled on the same grid as the observations (Extended Data Fig. 5 shows 5 × MWS). The mean correlation of the simulated anomalies with observations is improved by adding the wind and meltwater perturbations: from 0.27 ± 0.04 in the standard scenario to 0.44 ± 0.04 in the WMS (and 0.43 ± 0.01 in the 5 × WMS). The WMS simulates significant isopycnal deepening between 60° and 30° S throughout the whole upper 2,000 m, where waters are warming and freshening, similar to the observations in Fig. 1. Where the isopycnals deepen in the upper 1,000 m, the MWS simulates relatively reduced nitrate and DIC concentrations, increased oxygen concentrations and a shallower decrease in pH.

While ventilation is reduced north of 30° S, between 60° S and 30° S, the WMS simulates a decrease in ocean age relative to the standard scenario where isopycnals deepen (Fig. 5). We therefore attribute changes in ocean age and biogeochemistry north of 60° S to wind perturbation, driving increased ventilation in the subsurface ocean.

South of 60° S, the wind–meltwater perturbations cause an increase in simulated subsurface temperature, salinity and nitrate and DIC concentrations, and a reduction in oxygen concentrations and pH, consistent with Figs. 1 and 2. This simulated temperature and salinity response is also partly present in the wind-only experiment (Extended Data Fig. 8), which simulates an increase in ventilation in these regions. A poleward shift of the westerly winds causes a reduction of the easterly winds around the Antarctic coast. Easterly winds around Antarctica drive downwelling of waters through Ekman pumping, so a reduction in the easterlies leads to reduced downward Ekman pumping, and therefore upwelling of warm, saline and carbon-rich water[27]. However, meltwater is necessary to simulate the appropriate vertical structure of the observed changes. While the wind-only perturbations are required to produce the sign of anomalies observed, the wind increase leads to surface maxima. The meltwater is needed to reduce surface anomalies and cause the subsurface maxima (see Extended Data Figs. 4 and 7). While ref. [28] observed freshening along the bottom in some regions of the Antarctic shelf before 2013, the shallower increases in salinity and temperature that we observe are consistent with a recent influence of wind and meltwater.

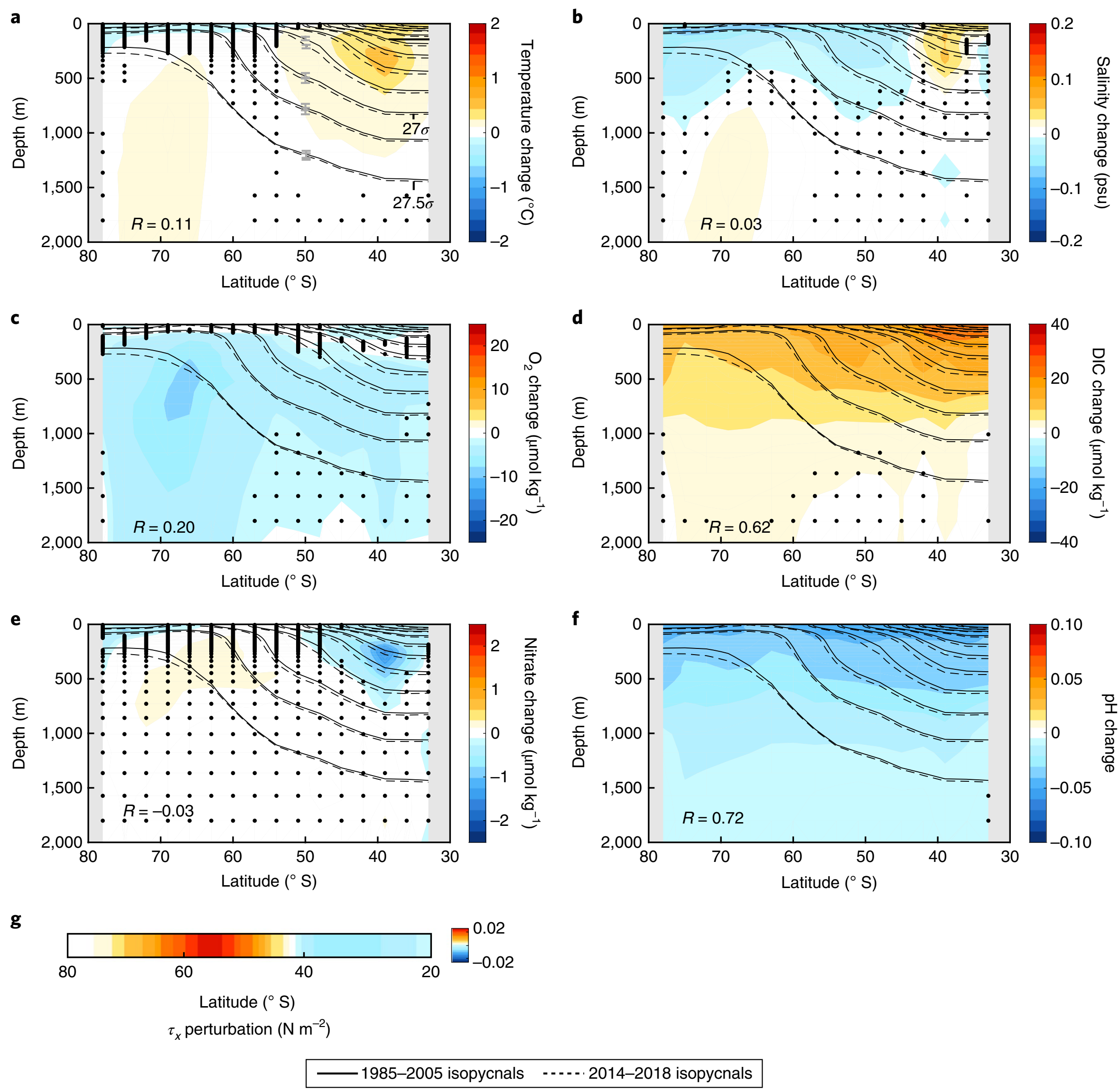

Fig. 3 | SS decadal changes. a–f, The five-member ensemble mean of the zonal mean differences in temperature (**a**), salinity (**b**), oxygen (**c**), DIC (**d**) and nitrate (**e**) concentrations and pH (**f**) between 2014–2019 and 1985–2005 in the standard RCP 8.5 ESM2M simulation, subsampled on the same grid as the observations. Solid and dashed lines show zonal mean 1985–2005 and 2014–2019 isopycnal surfaces, respectively. The grey error bars indicate the range of uncertainty in isopycnal depths, as diagnosed from 75 20-yr periods of a 1,500-yr pre-industrial ESM2M control simulation. The stippling indicates where the differences are not significant at the 90% level. *R* values in the bottom left corners of the maps give the correlation coefficient with the observed zonal mean changes in Figs. 1 and 2.

A wind-driven increase in the upwelling of warm, saline, low-oxygen circumpolar deep water, and a reduction in ocean ventilation around the Antarctic coast[8,29], lead to reductions in subsurface oxygen concentrations. The wind-driven decrease in downward Ekman pumping keeps older, deeper, oxygen-poor and carbon-rich water near the surface. The meltwater-driven reduction in ventilation causes an accumulation of ocean nutrients and carbon. The wind and meltwater effects on ventilation south of 60° S reinforce each other (Fig. 5). As these waters become isolated from the surface, more of the organic carbon is remineralized, leading to decreases in oxygen and pH. Refs. [8,30] also showed that the addition of Antarctic meltwater causes warming around the Antarctic continent, which reduces oxygen solubility. The coastal warming around Antarctica accounts for less than half of the observed oxygen anomaly, the rest being driven by a reduction in ocean ventilation due to both wind and meltwater changes (see Extended Data Fig. 6). We do not attribute these changes to variation in surface biological production, as the meltwater-only experiment simulates only a small reduction in surface biology and subsurface remineralization near the coast, inconsistent with the simulated changes in nitrate and oxygen concentrations.

Overall, compared with the SS, the WMS is more consistent with the observed decadal changes reported here. This is also true of the 5×WMS. However, both experiments simulate weak changes in temperature and salinity south of 60° S, which can be explained by the lack of a sharp Antarctic Slope Front (ASF) in ESM2M compared with observations. Small changes in the location of the ASF can lead to large changes in temperature due to the sharp gradients associated with the ASF[31,32]. The lack of an ASF in ESM2M may therefore reduce the model's sensitivity to wind and meltwater perturbations south of 60° S, explaining why the 5×WMS more closely matches the observations compared with the WMS (Extended Data Fig. 7).

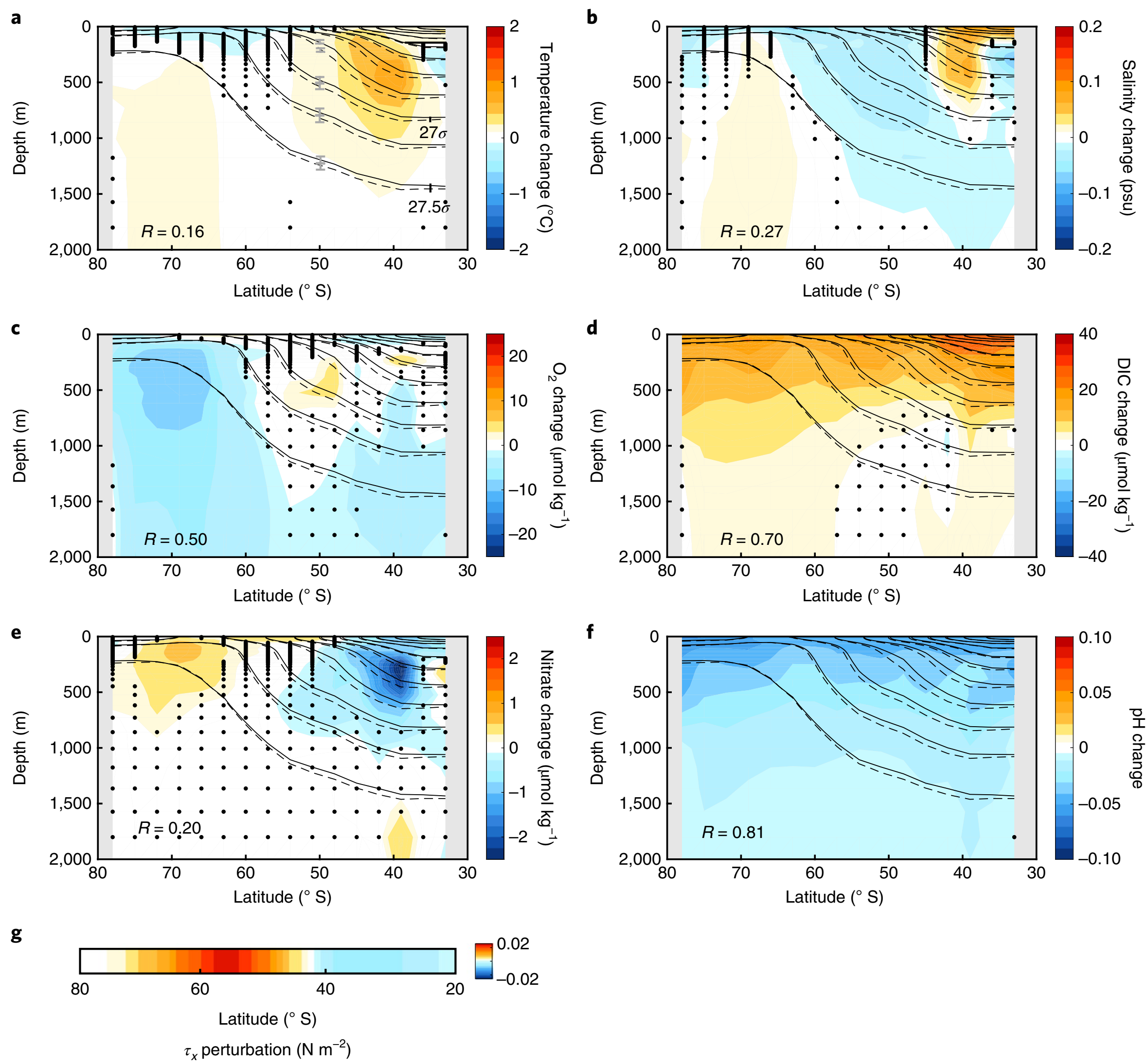

Fig. 4 | WMS decadal changes. a–f, The five-member ensemble mean of the zonal mean differences in temperature (**a**), salinity (**b**), oxygen (**c**), DIC (**d**) and nitrate (**e**) concentrations and pH (**f**) between 2005–2025 of the WM RCP 8.5 ESM2M simulation and 1985–2005 of the standard simulation, subsampled on the same grid as the observations. Solid and dashed lines show zonal mean 1985–2005 and 2014–2019 isopycnal surfaces, respectively. Panel **g** shows the applied Southern Ocean zonal wind stress perturbation, shown at the same latitudes as panels **a**-**d**. The grey error bars indicate the range of uncertainty in isopycnal depths, as diagnosed from 75 20-yr periods of a 1,500-yr pre-industrial ESM2M control simulation. The stippling indicates where the differences are significant at the 90% level. *R* values in the bottom left corners of the panels give the correlation coefficient with the observed zonal mean changes in Figs. 1 and 2.

However, we find a significant improvement in overall correlation with observed changes across both strengths of wind–meltwater perturbations, demonstrating that our conclusions do not depend on the magnitude of the added wind and meltwater (Extended Data Fig. 10). In both perturbation scenarios, we find that recent increases in wind strength and meltwater are important for simulating recent Southern Ocean changes.

Future impact of wind and meltwater

The observed warming around the Antarctic coast is largest in West Antarctica where the largest rates of ice shelf melting have been observed[9,10], supporting previous findings that meltwater discharge leads to subsurface warming[8,29,33]. However, we suggest that changes in easterly winds along the Antarctic coast, due to a poleward shift of the westerlies, contribute to observed coastal warming[27,32] (Extended Data Fig. 8). The large observed subsurface warming may lead to increased ice shelf and sheet melt, and therefore more sea-level rise[8]. However, the observed warming at 400 m depth, used as the relevant depth for ice shelf melt in ref. [34], is greater than previously observed or simulated[8,34]. The observed warming suggests that sub-ice-shelf melt in Antarctica may be underestimated in projections of Antarctic ice sheet melt and its contribution to sea-level rise.

Wind and meltwater have opposing effects on Southern Ocean biogeochemistry. Meltwater causes a reduction in ventilation: poorer ventilation acts to decrease subsurface oxygen while also increasing subsurface nitrate concentrations through the accumulation of nutrients in more poorly ventilated waters and reduced nitrate export out of the Southern Ocean. The reduction in nitrate concentrations therefore propagates to low latitudes. In opposition, the wind-induced increase in ventilation causes an increase in oxygen cocentrations throughout the upper 1,000 m of the Southern Ocean, while at the same time increasing surface nutrients through increased upwelling of deep, nutrient-rich waters[1]. The effects of wind and meltwater on ventilation can therefore influence future

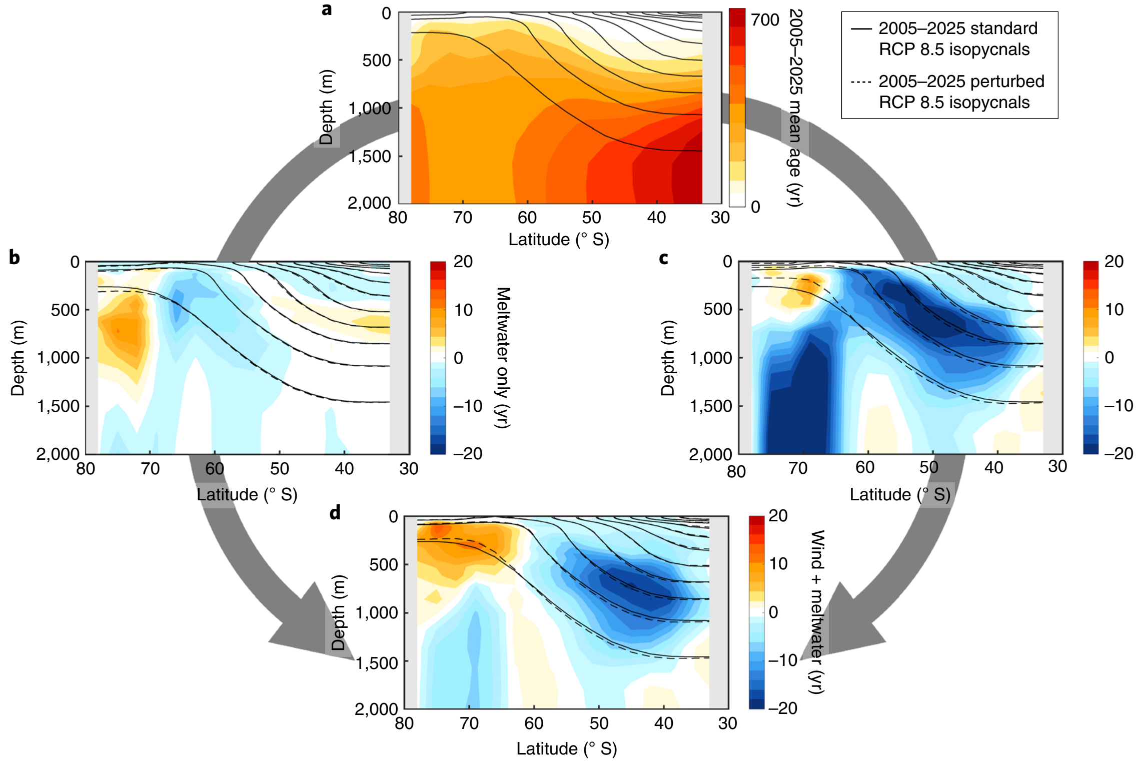

Fig. 5 | Ocean ventilation changes. a, The 2005–2025 zonal mean ocean age under the standard RCP 8.5 scenario. **b**–**d**, Zonal mean change in ocean age due to the applied meltwater (**b**), wind (**c**) and simultaneous wind and meltwater (**d**) perturbations in the wind-only, meltwater-only and wind–meltwater experiments, respectively. Anomalies in **b**–**d** are calculated with respect to the 2005–2025 mean of the standard RCP 8.5 scenario. An increase in ocean age indicates reduced ventilation, whereas a decrease in age indicates increased ventilation. The model is not subsampled.

projections of ocean biogeochemistry. The WMS is designed to match historical wind and melt changes, so we use the 5 × WMS to assess potential future impacts.

Figure 6 shows timeseries of upper-1,000-m oxygen and nitrate anomalies in the SS, 5 × WMS, 5 × wind-only and 5 × meltwater-only simulations south of 60° S and between 60° S and the Equator. For reference, Fig. 6 also shows anomalies that arise from applying RCP 8.5 projected Antarctic meltwater to the ESM2M simulation[34], as was done in ref. [8]. South of 60° S, the wind response dominates the combined effects of wind and meltwater, driving an increase in oxygen concentrations. This is exacerbated north of 60° S, where the effect of meltwater is even smaller, leading to an overall larger WMS increase in oxygen relative to the south.

We acknowledge that the perturbations we apply are idealized and designed to demonstrate the patterns that arise from accounting for wind and meltwater forcings. In the real atmosphere, the inferred poleward intensification of the winds is partly due to greenhouse gas forcing (which is expected to continue[35]) and partly due to the expansion of the ozone hole (which is expected to recover over the next few decades)[36,37]. However, the magnitude of Antarctic meltwater is expected to increase up to 0.6 Sv by the end of the century[34]. In the future, we might therefore expect the effect of meltwater on the Southern Ocean to become increasingly dominant compared with the poleward intensification of the westerlies.

Future climate change beyond 2100 is expected to cause nutrient trapping in the Southern Ocean through increases in surface stratification and poleward-shifting westerlies, starving the world-wide ocean of nutrients[38,39]. We find that adding meltwater strongly amplifies Southern Ocean nutrient accumulation south of 60° S, while both wind and meltwater lead to decreased nutrients north of 60° S (Fig. 6). While Southern Ocean nutrient trapping is found to be important in the twenty-second century[39], our results suggest that accounting for Antarctic meltwater and wind can cause similar effects in the twenty-first century, suppressing global biological productivity sooner than otherwise expected.

ESM2M is a coarse-resolution model, which limits reproduction of the structure of the observed physical and biogeochemical anomalies, particularly around the Antarctic coast (such as biases in the ASF, as discussed above). The model resolution may also influence the region where isopycnals deepen. In the ESM2M wind–meltwater simulations, isopycnals deepen most between 50 and 40° S throughout the whole water column. However, the observed isopycnals deepen most between 60 and 50° S. In part, this may be due to biases in its mean state density structure or parameterized mesoscale eddies, which respond differently to wind forcing if they are fully resolved[15,38,40,41]. However, comparisons between resolved and parameterized eddy models are often complicated due to different background states[41], so while we cannot attribute the difference in location of simulated and observed isopycnal deepening to model resolution, the resolution is probably important.

One study[5] found that the observed Southern Ocean temperature and salinity changes between the periods 1950–1980 and 2005–2015, largely driven by surface warming and freshening, are captured by climate model simulations. Despite using a later base period, our observed changes in salinity and temperature between 2014–2019 and the 1990s are larger than those between 2005–2015 and 1950–1980. This difference may be due to accelerating greenhouse gas forcing. However, observational estimates show a significant increase in Southern Ocean wind strength (as measured by the Southern Annular Mode index[42]) and in Antarctic ice sheet melt[10] over the past decade, which may further explain differences between our results and those of ref. [5]. More targeted quantitative

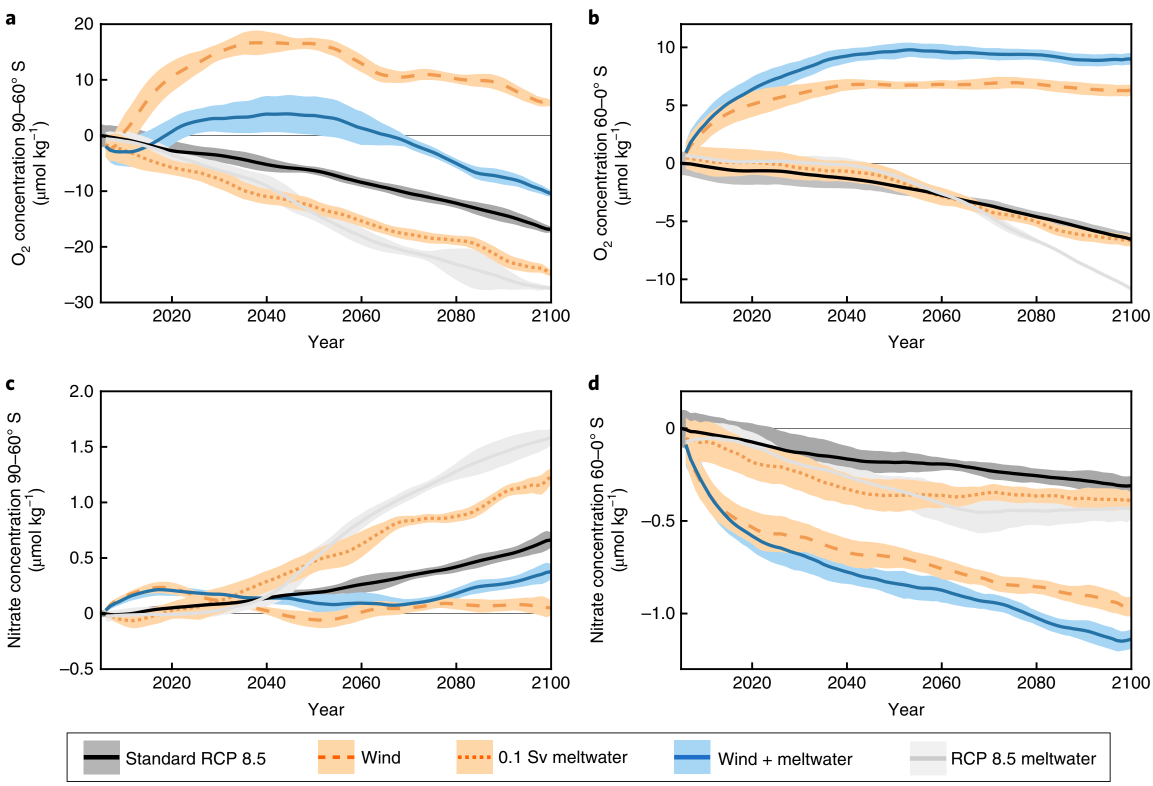

Fig. 6 | Future impact of wind and meltwater. a–d, Time series of ocean oxygen concentrations south of 60° S (**a**) and between 60° and 0° S (**b**) and nitrate concentrations south of 60° S (**c**) and between 60° and 0° S (**d**) in the upper 1,000 m relative to the 2014–2019 mean. The solid lines show the 10-yr-smoothed five-member ensemble means and the shading shows the 90% uncertainty range as diagnosed from the ensemble spread. The light grey shows anomalies that arise from applying RCP 8.5 projected Antarctic meltwater, similar to ref. [8].

further study should assess how well different models capture the observed changes.

Online content

Any methods, additional references, Nature Research reporting summaries, source data, extended data, supplementary information, acknowledgements, peer review information; details of author contributions and competing interests; and statements of data and code availability are available at https://doi.org/10.1038/s41561-019-0502-8.

Received: 7 January 2019; Accepted: 8 November 2019;
Published online: 6 January 2020

References

1. Marinov, I., Gnanadesikan, A., Toggweiler, J. & Sarmiento, J. The Southern Ocean biogeochemical divide. *Nature* **441**, 964–967 (2006).
2. Russell, J. L., Dixon, K. W., Gnanadesikan, A., Stouffer, R. J. & Toggweiler, J. R. The Southern Hemisphere westerlies in a warming world: propping open the door to the deep ocean. *J. Clim.* **19**, 6382–6390 (2006).
3. Boening, C. W., Dispert, A., Visbeck, M., Rintoul, S. R. & Schwarzkopf, F. U. The response of the Antarctic Circumpolar Current to recent climate change. *Nat. Geosci.* **1**, 864–869 (2008).
4. Armour, K. C., Marshall, J., Scott, J. R., Donohoe, A. & Newsom, E. R. Southern Ocean warming delayed by circumpolar upwelling and equatorward transport. *Nat. Geosci.* **9**, 549 (2016).
5. Swart, N. C., Gille, S. T., Fyfe, J. C. & Gillett, N. P. Recent Southern Ocean warming and freshening driven by greenhouse gas emissions and ozone depletion. *Nat. Geosci.* **11**, 836–841 (2018).
6. Swart, N. C. & Fyfe, J. C. Observed and simulated changes in the southern hemisphere surface westerly wind-stress. *Geophys. Res. Lett.* **39**, L16711 (2012).
7. Gillett, N. P. & Fyfe, J. C. Annular mode changes in the CMIP5 simulations. *Geophys. Res. Lett.* **40**, 1189–1193 (2013).
8. Bronselaer, B. et al. Change in future climate due to Antarctic meltwater. *Nature* **564**, 53–58 (2018).
9. Rignot, E., Jacobs, S., Mouginot, J. & Scheuchl, B. Ice-shelf melting around Antarctica. *Science* **341**, 266–270 (2013).
10. Shepherd, A. et al. Mass balance of the Antarctic Ice Sheet from 1992 to 2017. *Nature* **558**, 219–222 (2018).
11. Stouffer, R. J., Seidov, D. & Haupt, B. J. Climate response to external sources of freshwater: North Atlantic versus the Southern Ocean. *J. Clim.* **20**, 436–448 (2007).
12. Le Quere, C. et al. Saturation of the Southern Ocean CO_2 sink due to recent climate changes. *Science* **22**, 1735–1738 (2007).
13. Lovenduski, N. S., Gruber, N. & Doney, S. C. Toward a mechanistic understanding of the decadal trends in the Southern Ocean carbon sink. *Glob. Biogeochem. Cycles* **22**, GB3016 (2008).
14. Lovenduski, N. & Ito, T. The future evolution of the Southern Ocean CO_2 sink. *J. Mar. Res.* **67**, 597–617 (2009).
15. Jones, D. C., Ito, T. & Lovenduski, N. S. The transient response of the Southern Ocean pycnocline to changing atmospheric winds. *Geophys. Res. Lett.* **38**, L15604 (2011).
16. Bronselaer, B., Zanna, L., Munday, D. & Lowe, J. The influence of Southern Ocean winds on the North Atlantic carbon sink. *Glob. Biogeochem. Cycles* **30**, 844–858 (2016).
17. Khatiwala, S., Primeau, F. & Hall, T. Reconstruction of the history of anthropogenic CO_2 concentrations in the ocean. *Nature* **462**, 346–349 (2009).
18. Levitus, S. et al. World ocean heat content and thermosteric sea level change (0-2000m) 1955–2010. *Geophys. Res. Lett.* **39**, L10603 (2012).
19. Toggweiler, J. R. Shifting westerlies. *Science* **323**, 1434–1435 (2009).
20. Abernathey, R., Marshall, J. & Ferreira, D. The dependence of Southern Ocean meridional overturning on wind stress. *J. Phys. Oceanogr.* **41**, 2261–2278 (2011).
21. Lauderdale, J. M., Garabato, A. C. N., Oliver, K. I. C., Follows, M. J. & Williams, R. G. Wind-driven changes in Southern Ocean residual circulation, ocean carbon reservoirs and atmospheric CO_2. *Clim. Dynam.* **41**, 2145–2164 (2013).
22. *Argo Float Data and Metadata from Global Data Assembly Centre (Argo GDAC)* (SEANOE, 2018).

23. Gille, S. Warming of the Southern Ocean since the 1950s. *Science* **295**, 1275–1277 (2002).
24. Oschlies, A., Brandt, P., Stramma, L. & Schmidtko, S. Drivers and mechanisms of ocean deoxygenation. *Nat. Geosci.* **11**, 467–473 (2018).
25. Olsen, A. et al. The global ocean data analysis project version 2 (GLODAPv2)—an internally consistent data product for the world ocean. *Earth Syst. Sci. Data* **8**, 297–323 (2016).
26. Fay, A. R. et al. Utilizing the Drake Passage time-series to understand variability and change in subpolar Southern Ocean pCO_2. *Biogeosciences* **15**, 3841–3855 (2018).
27. Spence, P. et al. Rapid subsurface warming and circulation changes of Antarctic coastalwaters by poleward shifting winds. *Geophys. Res. Lett.* **41**, 4601–4610 (2014).
28. Schmidtko, S., Heywood, K. J., Thompson, A. F. & Aoki, S. Multidecadal warming of Antarctic waters. *Science* **346**, 1227–1231 (2014).
29. Fogwill, C. J., Phipps, S. J., Turney, C. S. M. & Golledge, N. R. Sensitivity of the Southern Ocean to enhanced regional Antarctic ice sheet meltwater input. *Earth Future* **3**, 317–329 (2015).
30. Fogwill, C. J. et al. Antarctic ice sheet discharge driven by atmosphere-ocean feedbacks at the last glacial termination. *Sci. Rep.* **7**, 39979 (2017).
31. Goddard, P. B., Dufour, C. O., Yin, J., Griffies, S. M. & Winton, M. CO_2-induced ocean warming of the Antarctic continental shelf in an eddying global climate model. *J. Geophys. Res. Oceans* **122**, 8079–8101 (2017).
32. Spence, P. et al. Localized rapid warming of West Antarctic subsurface waters by remote winds. *Nat. Clim. Change* **7**, 595–603 (2017).
33. Silvano, A. et al. Freshening by glacial meltwater enhances melting of ice shelves and reduces formation of Antarctic Bottom Water. *Sci. Adv.* **4**, eaap9467 (2018).
34. DeConto, R. M. & Pollard, D. Contribution of Antarctica to past and future sea-level rise. *Nature* **531**, 591–597 (2016).
35. Bracegirdle, T. J. et al. Assessment of surface winds over the Atlantic, Indian and Pacific Ocean sectors of the Southern Ocean in CMIP5 models: historical bias, forcing response and state dependence. *J. Geophys. Res.* **118**, 547–562 (2013).
36. Cionni, I. et al. Ozone database in support of CMIP5 simulations: results and corresponding radiative forcing. *Atmos. Chem. Phys.* **11**, 11267–11292 (2011).
37. Dhomse, S. S. et al. Estimates of ozone return dates from Chemistry-Climate Model Initiative simulations. *Atmos. Chem. Phys.* **18**, 8409–8438 (2018).
38. Munday, D. R., Johnson, H. L. & Marshall, D. P. Eddy saturation of equilibrated circumpolar currents. *J. Phys. Oceanogr.* **43**, 507–532 (2013).
39. Moore, J. K. et al. Sustained climate warming drives declining marine biological productivity. *Science* **359**, 1139–1143 (2018).
40. Farneti, R. & Delworth, T. L. The role of mesoscale eddies in the remote oceanic response to altered Southern Hemisphere winds. *J. Phys. Oceanogr.* **40**, 2348–2354 (2010).
41. Poulsen, M. B., Jochum, M. & Nuterman, R. Parameterized and resolved Southern Ocean eddy compensation. *Ocean Model.* **124**, 1–15 (2018).
42. Lin, X., Zhai, X., Wang, Z. & Munday, D. R. Mean, variability, and trend of Southern Ocean wind stress: role of wind fluctuations. *J. Clim.* **31**, 3557–3573 (2018).
43. Kanamitsu, M. et al. NCEP-DOE AMIP-II reanalysis (R-2). *Bull. Am. Meteorol. Soc.* **83**, 1631–1643 (2002).
44. Dee, D. P. et al. The ERA-Interim reanalysis: configuration and performance of the data assimilation system. *Q. J. R. Meteorol. Soc.* **137**, 553–597 (2011).

Publisher's note Springer Nature remains neutral with regard to jurisdictional claims in published maps and institutional affiliations.

Methods

Observational data. The SOCCOM dataset used in this study is constructed from all of the available biogeochemical float data since the start of the SOCCOM programme from January 2014 up to and including March 2019, and includes data from 146 floats. The floats directly measure nitrate and oxygen concentrations and pH, while DIC concentrations are derived from float-measured pH and an estimate for total alkalinity. Information about the quality control methods can be found in ref. [45]. The accuracies of temperature, salinity, nitrate, oxygen and pH data are ±0.002 °C, ±0.005 psu, 0.5 ± 0.5 μmol kg^{-1}, 1 ± 1% and 0.01 ± 0.007, respectively[46,47], and the accuracy of float-derived DIC is 5.5 ± 6.4 μmol kg^{-1} (refs. [45,47]) (quoted as $\sigma_{systematic} \pm \sigma_{random}$, see below for definitions). Carbon system parameters are calculated using the locally Iinterpolated alkalinity regression (LIARv2)[48]; the differences in DIC derived using the LIAR and multiple linear regression (MLR) products[49] are within our stated errors. Biogeochemical variables are sampled at a lower vertical resolution than temperature, salinity and pressure (referred to here as low-resolution SOCCOM data). We therefore use low-resolution temperature and salinity variables for consistency. We address uncertainties due to higher-resolution temperature and salinity data in our error analysis (see below).

The SOCCOM data are gridded onto an 8° × 3° horizontal grid and across 23 vertical levels. We use an oblique cell since the correlation lengthscale in the Southern Ocean is longer in the zonal than the meridional direction[50]. Within each of these grid cells, we average all available float data into monthly means for each year in the January 2014 to April 2019 period and then quantify the temporal mean by averaging over all months. We use only quality-controlled float data with a quality flag of '0 = good'. While more temperature, salinity and oxygen measurements are available from seal and Argo data, we only use SOCCOM float data in the main text for consistency across all variables examined. We verify that SOCCOM float coverage gives an accurate representation of the observed changes by applying the procedure to a dataset of both Argo and SOCCOM float temperature and salinity measurements. The Argo dataset has higher spatial and temporal coverage than the SOCCOM dataset: 429 8° × 3° grid boxes are covered by Argo and SOCCOM combined, but only 284 are covered by the SOCCOM-only dataset. The addition of Argo data to the SOCCOM dataset mostly increases coverage South of 60° S and North of 50° S (see Extended Data Fig. 1). Yet, unlike Argo, SOCCOM floats provide biogeochemical information and have the unique ability to sample under sea ice. The observed differences between the shipboard and the combined Argo/SOCCOM dataset are shown in Extended Data Fig. 1, and show good comparison with the SOCCOM-only anomalies in Fig. 1. The spatial correlations between the two comparisons are 0.79 and 0.72 for temperature and salinity, respectively, giving confidence in the use of the SOCCOM data for the biogeochemical anomalies.

For the observational estimate before 2005, we use the adjusted shipboard data from the GLODAPv2 synthesis product[25]. We only use data south of 30° S, spanning the period from 1985 to 2005, and with an 'acceptable' quality flag (flag number 2), as well duplicate good data (flag number 6). This filtering process results in 6,545 hydrographic stations. Typical uncertainty (σ_{random}, we assume there is no systematic error) in shipboard bottle measurements of salinity, nitrate, DIC and oxygen concentrations are 0.005 psu, 2 %, 4 μmol kg^{-1}, 1% and 0.005 μmol kg^{-1}, respectively[25]. The pH values in the GLODAPv2 shipboard bottle dataset are either directly measured or calculated from bottle measurements of DIC and total alkalinity, pH(DIC,TA). Where pH is directly measured, it is adjusted during the GLODAPv2 QC process by a cruise-dependent offset to be consistent with pH(DIC,TA). We use these internally consistent GLODAPv2 pH values reported at in situ pressure and temperature[25]. To compare the GLODAPv2 shipboard pH dataset with the in situ measured pH from the SOCCOM dataset, we apply the following correction from ref. [51] to the shipboard pH:

$$pH_{measured} = pH_{calculated} - 0.3168 + 0.0404 \times pH_{calculated} \quad (1)$$

This adjustment accounts for a known pH-dependent offset between directly measured pH (SOCCOM) and pH calculated from other carbonate system parameters (GLODAPv2)[48]. In our comparison, this adjustment mainly reduces the observed pH change below 1,500 m depth. Similar to the SOCCOM dataset, we average all available profile data in each 8° × 3° horizontal grid cell, and interpolate onto 23 vertical levels to match the SOCCOM data. While SOCCOM data are taken throughout the year, most shipboard measurements are taken in Austral summer, between December and May. The shipboard data is therefore biased towards the summer. To remove this seasonal bias, we calculate the differences between the December–May and annual and zonal means of the SOCCOM dataset, and subtract this from the shipboard data (see Extended Data Fig. 9). Most grid cells do not have data for all 12 months of the year, so we calculate the seasonal bias of the zonal mean.

The decadal changes reported in this study, calculated as the difference between the SOCCOM and shipboard datasets, are only calculated where the two datasets overlap in space. The spatial maps shown in Extended Data Fig. 2 of the 0–1,000 m mean decadal changes in nitrate, DIC and oxygen concentrations and pH show the spatial distribution of this overlap. The observational uncertainties shown in the figures are discussed below in Significance testing.

ESM2M. ESM2M is an Earth system model from the CMIP5 ensemble. It has a coupled carbon cycle and has a 1° × 1° horizontal ocean model resolution with increased resolution near the Equator and 50 unevenly spaced vertical levels in depth coordinates. The ocean model has a free surface[51,52] and parameterized mesoscale eddies using the GM-Redi schemes[53]. The Southern Ocean in ESM2M has relatively deep mixed layers compared with the overall CMIP5 mean, but it is not an outlier within the CMIP5 ensemble[54].

The Southern Ocean mixed layer depth response to climate change scenarios in ESM2M is relatively weak compared with the overall CMIP5 mean[54]; ref. [55] shows that there is a large spread in winter-time mixed layer patterns and convection. However, ESM2M has deep mixed layers in areas that correspond to the observations. Winter-time open-ocean convection and polynya formation in ESM2M is confined to the Eastern Weddell sea[54], similar to observed open-ocean polynyas in the 1970s and in recent years[55,56]. Observations also show deep mixed layers around the Antarctic coast, where dense water is thought to form. ESM2M simulates deeper mixed layers around the coast, however, these mixed layers are shallower than those observed[57], which may be due to a lack of sharp ASF in ESM2M. The density structure of ESM2M around the Antarctic coast is evaluated in ref. [8]. Overall, ESM2M demonstrates good climate fidelity[51] and has been shown to perform well in terms of global and Southern Ocean heat uptake[58].

The ocean biogeochemistry and ecology in ESM2M are calculated using the tracers of ocean phytoplankton with allometric zooplankton code version 2 (TOPAZ2), discussed in detail in refs. [52,59,60]. TOPAZ2 uses 30 tracers to calculate changes in carbon, nitrogen, phosphorous, silicon, iron and oxygen concentrations and alkalinity and lithogenic material. The ESM2M biogeochemical fields have relatively low biases in Southern Ocean nutrient and oxygen distributions[52].

Wind stress and meltwater perturbations. To demonstrate the interaction of poleward-intensifying winds and meltwater discharge, we use idealized forcing profiles and apply the perturbations as steps during the years 2005 to 2025 to each of the five ensemble members of the SS. The main reason is the uncertainty in historical, and by extension, future trends in Southern Ocean westerly winds and Antarctic ice melt. While reanalysis products are commonly used for historical surface ocean wind stress, the trend in the Southern Ocean wind stress varies significantly between different products. For example, the 1979–2018 NCEP R2 yearly linear trend in maximum wind stress multiplied by 39 years, 0.053 N m^{-2}, is more than double that of ERA-interim[42], (0.025 N m^{-2}). Ref. [47] shows that CMIP5 models strongly underestimate historical wind stress trends com- pared to all reanalysis products. The change in maximum wind stress of the 5-member ESM2M ensemble is 0.0107 ± 0.003 N m^{-2}, by the same metric. By comparison, the change in the 14 CMIP5 models used in ref. [61] is 0.012 ± 0.013 N m^{-2}, so ESM2M is a suitable representative of the CMIP5 mean. CMIP5 models are therefore missing a large climate change-induced forcing that we aim to account for. One could force ESM2M to simulate the historical linear trend in wind stress from a reanalysis product through a flux adjustment and extrapolate this into the future. However, this requires a choice that would quantitatively impact the results. Therefore, we address the qualitative impact of poleward-intensifying winds by focusing on the spatial patterns that result from an idealized poleward strengthening of the Southern Ocean westerlies.

We force a poleward intensification of the Southern Ocean winds by using the zonal mean of the momentum flux perturbation from the Flux-Anomaly-Forced Model Intercomparison Project (FAFMIP) south of 30° S. This momentum flux perturbation is the year 61–80 mean of the simulated zonal wind stress anomaly in 13 CMIP5 models under an idealized 1% CO_2 simulation performed by each model. Imposing this pattern on a pre-industrial control simulation causes a poleward intensification of the wind stress. The applied zonal wind stress anomaly is shown in Fig. 3g, and constitutes a 0.02 N m^{-2} (roughly 10%) increase in zonal mean wind stress and a 0.4° poleward shift of the position of the maximum zonal mean wind stress.

The uncertainty in projected meltwater from Antarctica over the next century is large, since the uncertainty range in the IPCC 2100 Antarctic contribution to sea-level rise is more than 100% of the mean projection[62]. As CMIP5 models lack ice sheet meltwater entirely, we prescribe a constant 0.02 Sv meltwater flux at the ocean's surface at sea surface temperature to represent ice sheet melt. This magnitude of projected Antarctic meltwater flux is first reached in the year 2017 of the ref. [34] Antarctic meltwater projection. The decadal changes simulated by the step meltwater perturbation are equivalent to those simulated in an ESM2M simulation with a transient meltwater flux taken from ref. [34], as used in ref. [8] (see Extended Data Fig. 4 and Supplementary Fig. 5). We impose the meltwater uniformly at the surface around the Antarctic coast, over the nearest 3° of latitude. Ref. [63] shows that adding the meltwater all at the surface does not significantly affect the total Antarctic sea ice response, but may affect regional sea ice trends. Spatial variation in the meltwater flux does not significantly affect the total sea ice extent response either[64], as freshwater anomalies are transported around the coast via the westward coastal current. However, applying the freshwater over a wider area around the coast to account for transport of freshwater by icebergs does affect the sea ice extent, which is why we have spread our freshwater flux over several gridboxes away from the coast.

However, to demonstrate that our conclusions do not depend on the choice of perturbation magnitudes, we also perform simulations with wind and meltwater that are five time larger than the ones discussed above. These larger perturbations therefore impose a 50% increase in zonal mean wind stress and a 2° poleward shift of the position of the maximum zonal mean wind stress, as well as a 0.1 Sv freshwater flux (this magnitude is first reached in the year 2037 of the projection in ref. [34]). We also apply these perturbations (separately and simultaneously) during the years 2005–2025 in five members of the standard ESM2M scenario individually.

Significance testing. Throughout the paper, we refer to signals being 'significant' if they are larger than the 90% confidence range, or 1.65σ; σ includes contributions from: (1) random error in the mean, $\sigma_{\rm random}$, this is calculated as the random error in the observational measurement and is divided by the number of data points used for the quantity shown, N (where N is the number of ship or float measurements used in the zonal mean, or in the vertical integral); (2) systematic error, $\sigma_{\rm systematic}$, this is taken as the estimated systematic error in the SOCCOM sensors; (3) uncertainty due to natural variability, $\sigma_{\rm variability}$, this is difficult to estimate from the limited observational record, so we estimate $\sigma_{\rm variability}$ as the standard deviation of the differences between the 1985–2005 and 2014–2019 means across a 30-member historical–RCP 8.5 ESM2M large ensemble simulation, as used in ref. [65] and ref. [8]. We calculate these differences on a 8°×3° horizontal grid, and only in grid cells where there is overlap between the SOCCOM and shipboard datasets (this overlap is different for each variable). This method assumes that the observed natural variability is similar to the ESM2M simulated natural variability. (4) Uncertainty due to interpolation, $\sigma_{\rm interpolation}$, when interpolating the observations onto the 23 vertical levels, we use four different interpolation methods: linear, nearest neighbour, spline and cubic. We use the mean of these four interpolation methods in our analysis. We then use the standard deviation of the differences between these methods divided by $(3-1)^{1/2}$ to get the error in the mean, $\sigma_{\rm interpolation}$. In the case of temperature and salinity, we repeat the procedure with the high-resolution SOCCOM data to get eight separate estimates. We divide the standard deviation of these 8 estimates by $(8-1)^{1/2}$ to get the error in the mean, $\sigma_{\rm interpolation}$. The errors are denoted with a subscript SOCCOM for the SOCCOM data, and GLODAP for the GLODAP data and are added in quadrature as these error are uncorrelated. The overall error, σ, is then given by the equation:

$$\sigma^2 = \sigma^2_{\rm variability} + \sigma^2_{\rm interpolation} + \sigma^2_{\rm systematic,SOCCOM} + \left(\sigma^2_{\rm random,GLODAP}/N_{\rm GLODAP} + \sigma^2_{\rm random,SOCCOM}/N_{\rm SOCCOM}\right) \quad (2)$$

For significance testing in the ESM2M ensemble simulations shown in Figs. 3 and 4, we test for a 90% confidence level. Differences are significant if they are larger than $1.65\sigma_{\rm variability}/(N-1)^{1/2}$. $\sigma_{\rm variability}$ is the estimated standard deviation of the difference between the 1985–2005 and 2014–2019 mean of the 30-member historical–RCP 8.5 ESM2M large ensemble simulation used in ref. [63] and ref. [10]. N is the number of ensemble members, so $N=5$ for all our experiments. We calculate these differences on a 8°×3° horizontal grid. Stippling is used when the simulated changes are less than $1.65\sigma_{\rm variability}/(N-1)^{1/2}$.

Decomposition of pH changes. Changes in pH can be driven by either increased carbon concentrations or changes in biological activity and ocean dynamics[66,67]. To understand the observed and simulated changes in pH, we use a set of idealized ESM2M model simulations with a 1% yr^{-1} increase in the partial pressure of atmospheric CO_2, p_{CO_2}, starting at 280 ppm. Atmospheric p_{CO_2} reaches double the initial value (that is, 560 ppm) after 70 years. In one simulation, the climate is fully coupled. In the second simulation, atmospheric carbon is treated as a non-radiative gas. This means that the radiative (or greenhouse gas) effect of CO_2 is disabled, similar to the simulations discussed in ref. [68].

Starting at an atmospheric p_{CO_2} level of 360 ppm (roughly the 1995 level), the 20-year change in zonal mean ocean pH is shown in Supplementary Fig. 6, for the fully coupled and non-radiative CO_2 simulations, respectively. Most of the simulated pH changes are caused by the intrusion of anthropogenic CO_2, rather than changes in dynamics or biology that arise as a result of ocean adaptations to atmospheric warming. This supports the evidence from observational correlations that the observed changes in pH are likely driven largely by changes in DIC concentrations.

Data availability

The SOCCOM data are available as a 12 March 2019 quality-controlled snapshot at https://doi.org/10.6075/J01G0JKT. The results from the standard, wind, meltwater and wind–meltwater RCP 8.5 simulations are freely available from the corresponding author. Shipboard data are available at https://odv.awi.de/data/ocean/glodap-v2-bottle-data/ and the GLODAP synthesis product is available at https://www.nodc.noaa.gov/ocads/oceans/GLODAPv2/. Argo data are available at http://www.Argodatamgt.org/.

Code availability

GFDL ESM2M model code is publicly available at https://github.com/mom-ocean.

References

45. Gray, A. R. et al. Autonomous biogeochemical floats detect significant carbon dioxide outgassing in the high-latitude Southern Ocean. *Geophys. Res. Lett.* **45**, 9049–9057 (2018).
46. Johnson, K. S. et al. Biogeochemical sensor performance in the SOCCOM profiling float array. *J. Geophys. Res. Oceans* **122**, 6416–6436 (2017).
47. Williams, N. L. et al. Assessment of the carbonate chemistry seasonal cycles in the Southern Ocean from persistent observational platforms. *J. Geophys. Res. Oceans* **123**, 4833–4852 (2018).
48. Carter, B. R. et al. Updated methods for global locally interpolated estimation of alkalinity, pH, and nitrate. *Limnol. Oceanogr. Methods* **16**, 119–131 (2018).
49. Williams, N. L. et al. Calculating surface ocean pCO$_2$ from biogeochemical Argo floats equipped with pH: an uncertainty analysis. *Glob. Biogeochem. Cycles* **31**, 591–604 (2017).
50. Mazloff, M. R., Cornuelle, B. D., Gille, S. T. & Verdy, A. Correlation lengths for estimating the large-scale carbon and heat content of the Southern Ocean. *J. Geophys. Res. Oceans* **123**, 883–901 (2018).
51. Dunne, J. P. et al. GFDL's ESM2 Global coupled climate-carbon Earth system models. Part I: physical formulation and baseline simulation characteristics. *J. Clim.* **25**, 6646–6665 (2012).
52. Dunne, J. P. et al. GFDL's ESM2 global coupled climate-carbon earth system models. Part II: carbon system formulation and baseline simulation characteristics. *J. Clim.* **26**, 2247–2267 (2013).
53. Griffies, S. The Gent-McWilliams skew flux. *J. Phys. Oceanogr.* **28**, 831–841 (1998).
54. Sallee, J. B. et al. Assessment of Southern Ocean water mass circulation and characteristics in CMIP5 models: historical bias and forcing response. *J. Geophys. Res. Oceans* **118**, 1830–1844 (2013).
55. Gordon, A. Deep Antarctic convection west of Maud Rise. *J. Phys. Oceanogr.* **8**, 600–612 (1978).
56. de Lavergne, C., Palter, J. B., Galbraith, E. D., Bernardello, R. & Marinov, I. Cessation of deep convection in the open Southern Ocean under anthropogenic climate change. *Nat. Clim. Change* **4**, 278–282 (2014).
57. Pellichero, V., Sallee, J.-B., Schmidtko, S., Roquet, F. & Charrassin, J.-B. The ocean mixed layer under Southern Ocean sea-ice: seasonal cycle and forcing. *J. Geophys. Res. Oceans* **122**, 1608–1633 (2017).
58. Froelicher, T. L. et al. Dominance of the Southern Ocean in anthropogenic carbon and heat uptake in CMIP5 models. *J. Clim.* **28**, 862–886 (2015).
59. Henson, S. A., Dunne, J. P. & Sarmiento, J. L. Decadal variability in North Atlantic phytoplankton blooms. *J. Geophys. Res. Oceans* **114**, C04013 (2009).
60. Dunne, J. P., Hales, B. & Toggweiler, J. R. Global calcite cycling constrained by sediment preservation controls. *Glob. Biogeochem. Cycles* **26**, GB3023 (2012).
61. Bronselaer, B., Winton, M., Russell, J., Sabine, C. L. & Khatiwala, S. Agreement of CMIP5 simulated and observed ocean anthropogenic CO_2 uptake. *Geophys. Res. Lett.* **44**, 12298–12305 (2017).
62. IPCC: Technical Summary. In *Climate Change 2013: The Physical Science Basis* (eds Stocker, T. F. et al.) (Cambridge Univ. Press, 2013).
63. Pauling, A. G., Bitz, C. M., Smith, I. J. & Langhorne, P. J. The response of the Southern Ocean and Antarctic sea ice to freshwater from ice shelves in an Earth system model. *J. Clim.* **29**, 1655–1672 (2016).
64. Haid, V., Iovino, D. & Masina, S. Impacts of freshwater changes on Antarctic sea ice in an eddy-permitting sea-ice-ocean model. *Cryosphere* **11**, 1387–1402 (2017).
65. Rodgers, K. B., Lin, J. & Froelicher, T. L. Emergence of multiple ocean ecosystem drivers in a large ensemble suite with an Earth system model. *Biogeosciences* **12**, 3301–3320 (2015).
66. Orr, J. et al. Anthropogenic ocean acidification over the twenty-first century and its impact on calcifying organisms. *Nature* **437**, 681–686 (2005).
67. Wootton, J. T., Pfister, C. A. & Forester, J. D. Dynamic patterns and ecological impacts of declining ocean pH in a high-resolution multi-year dataset. *Proc. Natl Acad. Sci. USA* **105**, 18848–18853 (2008).
68. Friedlingstein, P. et al. Climate-carbon cycle feedback analysis: results from the C4MIP model intercomparison. *J. Clim.* **19**, 3337–3353 (2006).

Acknowledgements

This work was sponsored by the NSF's SOCCOM Project under NSF Award No. PLR-1425989, with additional support from the NOAA and NASA. N.L.W. was supported by NOAA PMEL through the NRC post-doctoral programme and this is PMEL contribution no. 4834. Data were collected and made freely available by the SOCCOM Project funded by the National Science Foundation, Division of Polar Programs (NSF Award No. PLR -1425989), supplemented by NASA, and by the International Argo Program and the NOAA programmes that contribute to it (http://www.Argo.ucsd.edu, http://Argo.jcommops.org). The Argo Program is part of the Global Ocean Observing System. We thank the SOCCOM, Argo and GLODAP teams for making the data available online.

Author contributions

B.B. performed the simulations with help from J.L.R. and M.W. B.B., J.L.R. and M.W. analysed the data with help from N.L.W., R.M.K., R.A.F., K.S.J., J.L.S. (for observations) and J.P.D. (for simulations). All authors wrote the manuscript.

Competing interests

The authors declare no competing interests.

Additional information

Extended data is available for this paper at https://doi.org/10.1038/s41561-019-0502-8.

Supplementary information is available for this paper at https://doi.org/10.1038/s41561-019-0502-8.

Correspondence and requests for materials should be addressed to B.B.

Peer review information Primary Handling Editor: Xujia Jiang.

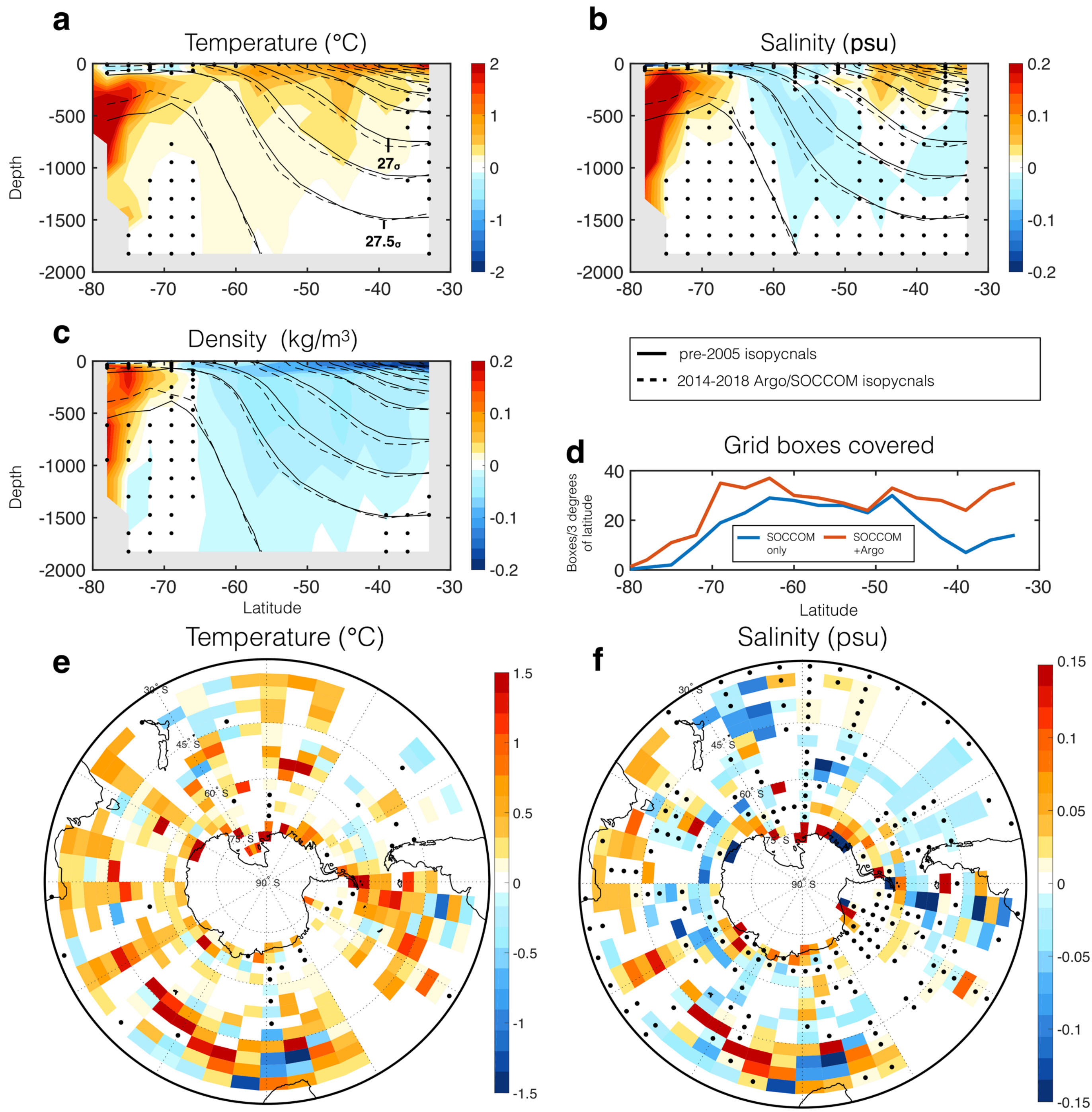

Extended Data Fig. 1 | Argo and SOCCOM anomalies. onal mean differences in **a**, temperature, **b**, salinity, and **c**, density between 2014–2019 combined Argo and SOCCOM data, and pre-2005 shipboard data. The comparison is only shown where there is overlap between both datasets on an 8x3° horizontal grid. Solid and dashed lines show zonal mean shipboard and Argo/SOCCOM isopycnal surfaces respectively. Grey shows areas with insufficient data. Panel **d** shows the number of grid boxes per 3 degrees of latitude covered by the SOCCOM data only and by the Argo+SOCCOM data in the shipboard comparison. The stippling indicates where the differences are not significant at the 90% level. Panels **e** and **f** show the upper 1000 m difference between Argo+SOCCOM and pre-2005 shipboard data for temperature and salinity respectively. The stippling indicates where the differences are not significant at the 90% level.

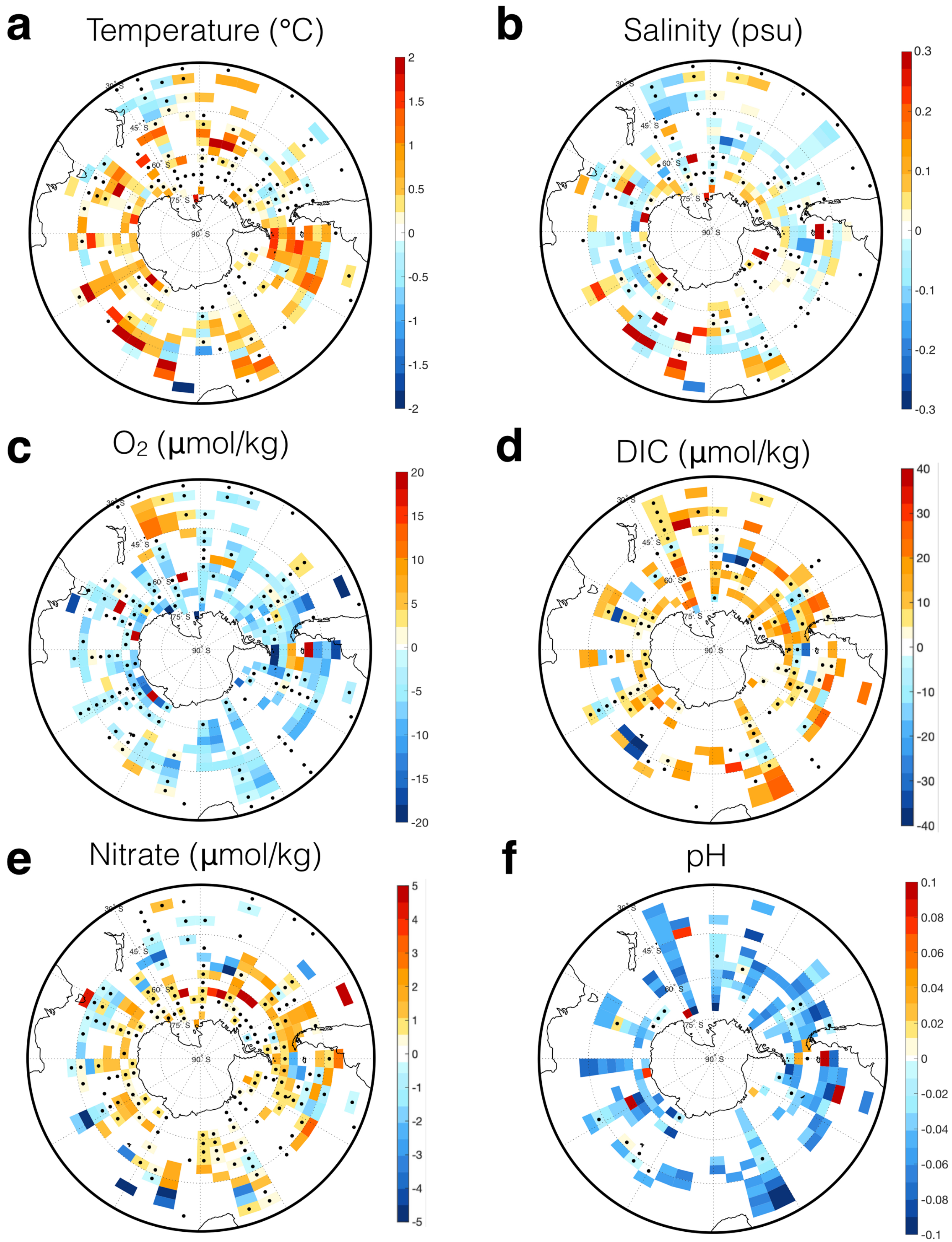

Extended Data Fig. 2 | Spatial coverage of data. upper 1000 m difference between SOCCOM and pre-2005 shipboard data for **a**, temperature, **b**, salinity, **c**, oxygen, **d**, dissolved inorganic carbon (DIC), **e**, nitrate and **f**, pH. All data was regridded onto a 8° × 3° horizontal grid prior to calculating differences. The stippling indicates where the differences are not significant at the 90% level.

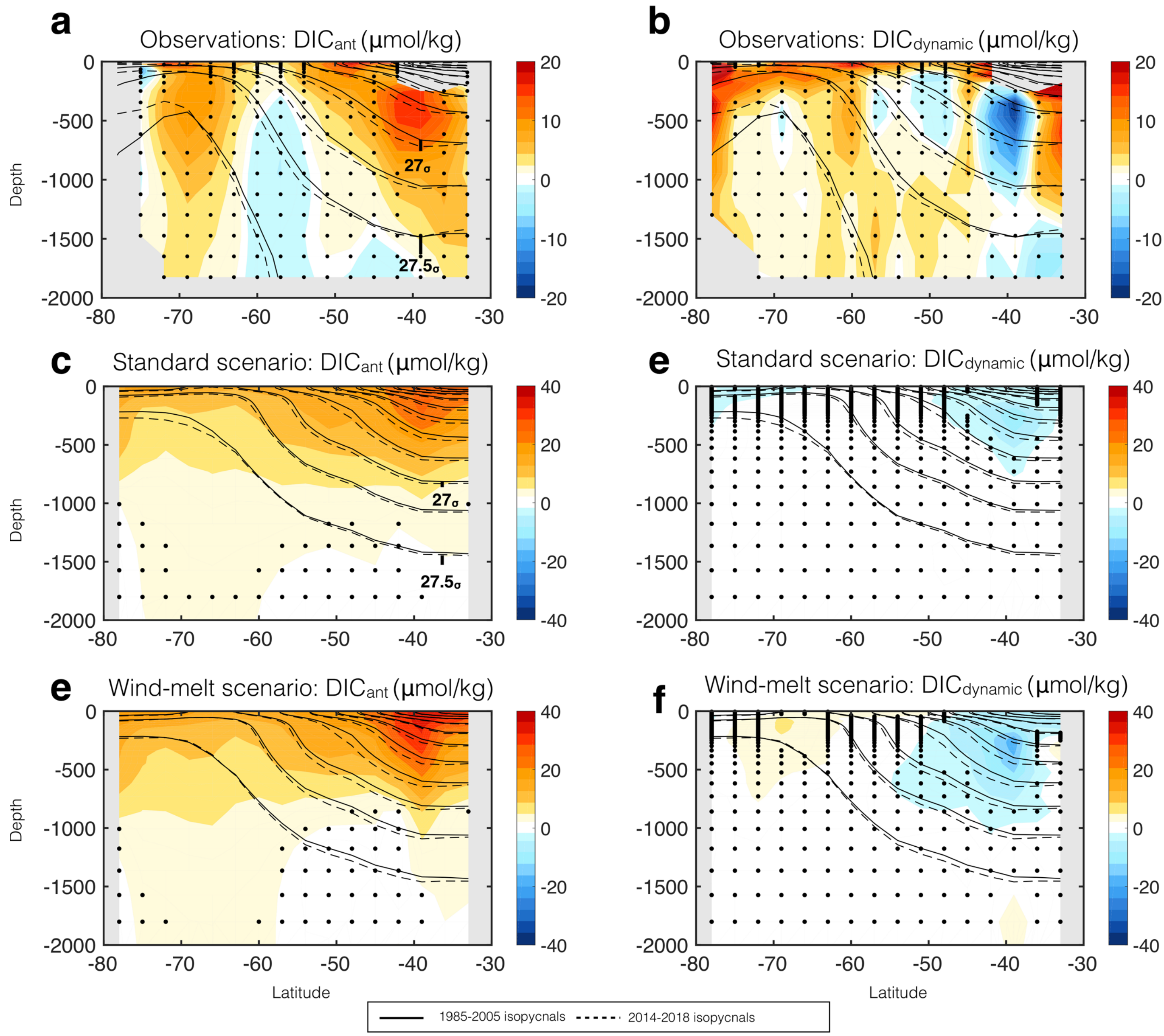

Extended Data Fig. 3 | Estimated anthropogenic and dynamical DIC changes. Panels **a**, **c** and **d** show the anthropogenic component of DIC changes, for the observations, standard ESM2M simulation and wind-meltwater simulation, respectively. The anthropogenic DIC change is calculated by subtracting 117/16 × dNO from the total change in DIC, where dNO is the change in Nitrate and 117/16 is the Redfield Ratio between carbon and nitrogen. Panels **b**, **e** and **f** show the dynamically-induced DIC changes, for the observations, standard ESM2M simulation and wind- meltwater simulation, respectively. The dynamically induced changes are calculated as 117/16 × dNO. We choose to use nitrate for this calculation since it less influenced by temperature than oxygen, and the simulated nitrate changes are inconsistent with the changes in surface biological productivity, meaning they are dominated by dynamics. A simple 2-degree smoothing has been applied to facilitate interpretation of large-scale patterns.

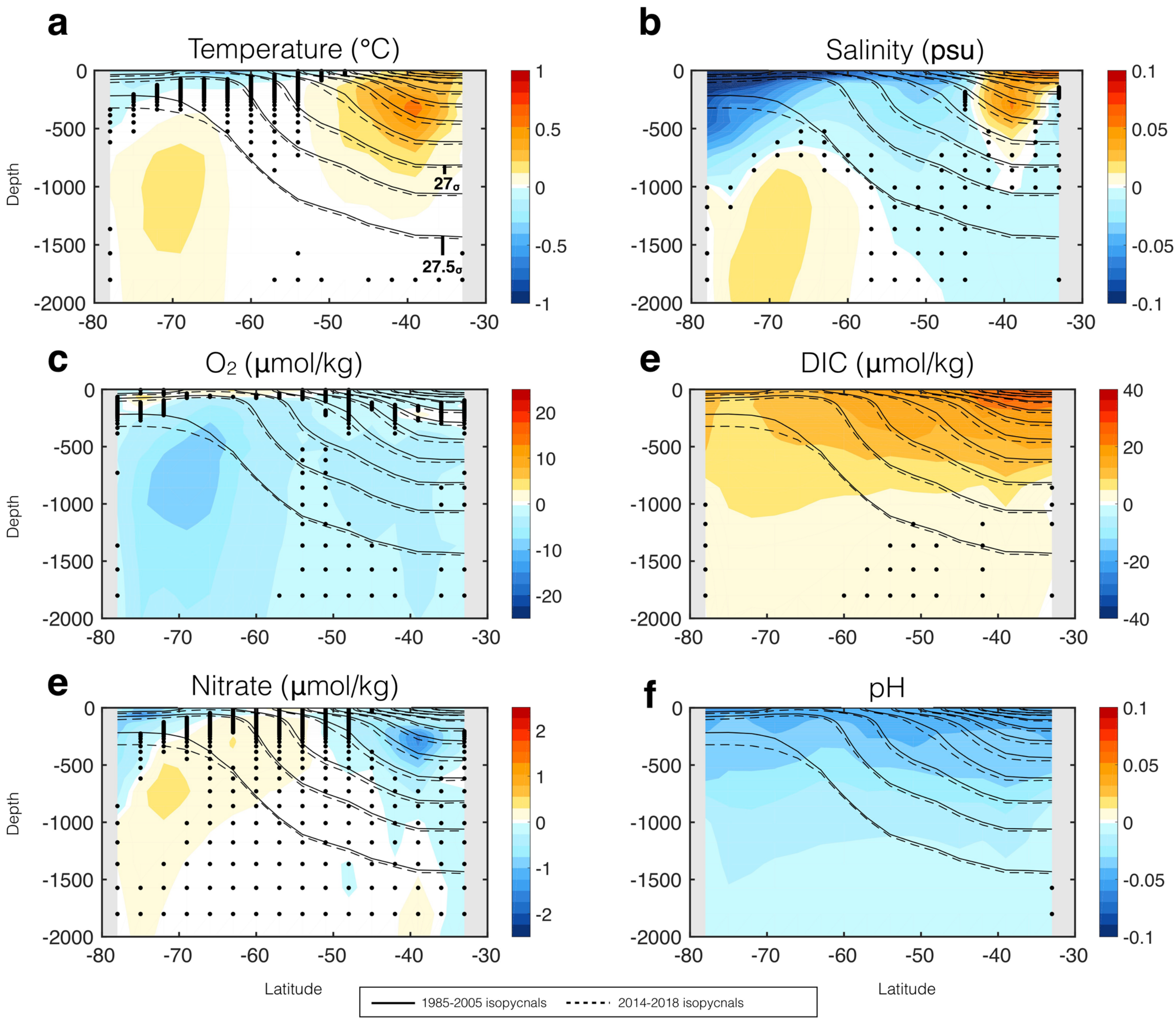

Extended Data Fig. 4 | Meltwater-only scenario simulated decadal changes. 5-member ensemble mean of the zonal mean differences in **a**, temperature, **b**, salinity, **c**, oxygen, **d**, dissolved inorganic carbon (DIC), **e**, nitrate and **f**, pH between years 2014-2019 of the meltwater-only RCP8.5 ESM2M simulation and years 1985–2005 of the standard simulation. Solid and dashed lines show zonal mean 1985–2005 and 2014–2019 isopycnal surfaces respectively. The stippling indicates where the differences are not significant at the 90% level (see Methods). Here, the model is not sub-sampled to show the whole Southern Ocean response to the added meltwater.

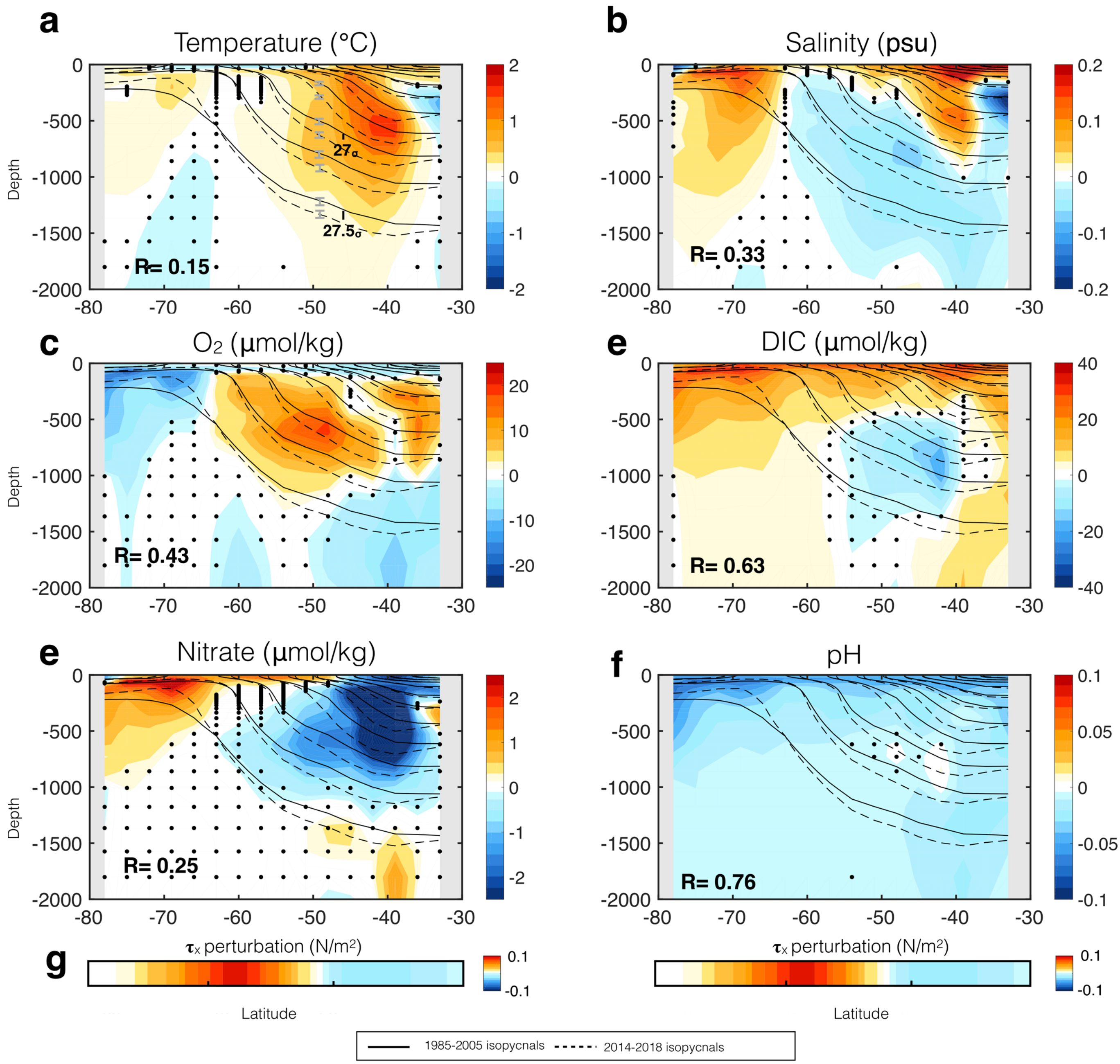

Extended Data Fig. 5 | 5×WM scenario simulated decadal changes. 5-member ensemble mean of the zonal mean differences in **a**, temperature, **b**, salinity, **c**, oxygen, **d**, dissolved inorganic carbon (DIC), **e**, nitrate and **f**, pH between years 2014-2019 of the 0.2×WMRCP8.5 ESM2M simulation and years 1985–2005 of the standard simulation, sub-sampled on the same grid as the observations. Solid and dashed lines show zonal mean 1985–2005 and 2014–2019 isopycnal surfaces respectively. The grey error bars indicate the range of uncertainty in isopycnal depths, as diagnosed from 75 20-years periods of a 1500-year pre-industrial ESM2M control simulation. The stippling indicates where the differences are significant at the 90% level. R-values in the bottom right corners of the panels give the correlation coefficient with the observed zonal mean changes in Figs. 1 and 2.

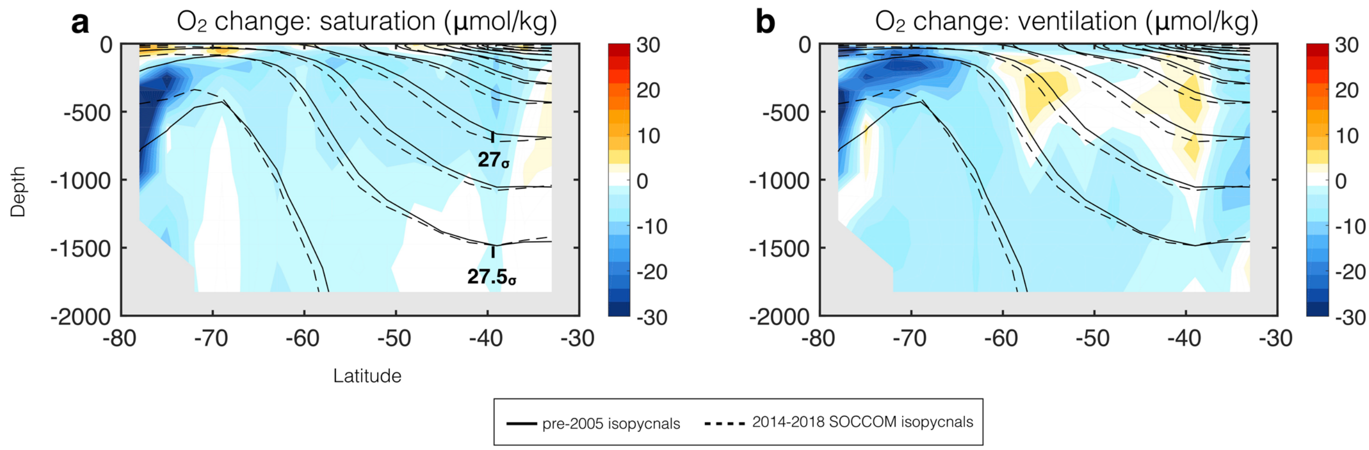

Extended Data Fig. 6 | Observed oxygen changes. zonal mean difference in oxygen due to **a**, changes in oxygen saturation (temperature-induced solubility change) and **b**, changes in ventilation and surface biological activity. The change due to ventilation and surface biology is calculated as the difference between the observed change in oxygen and the change in oxygen saturation.

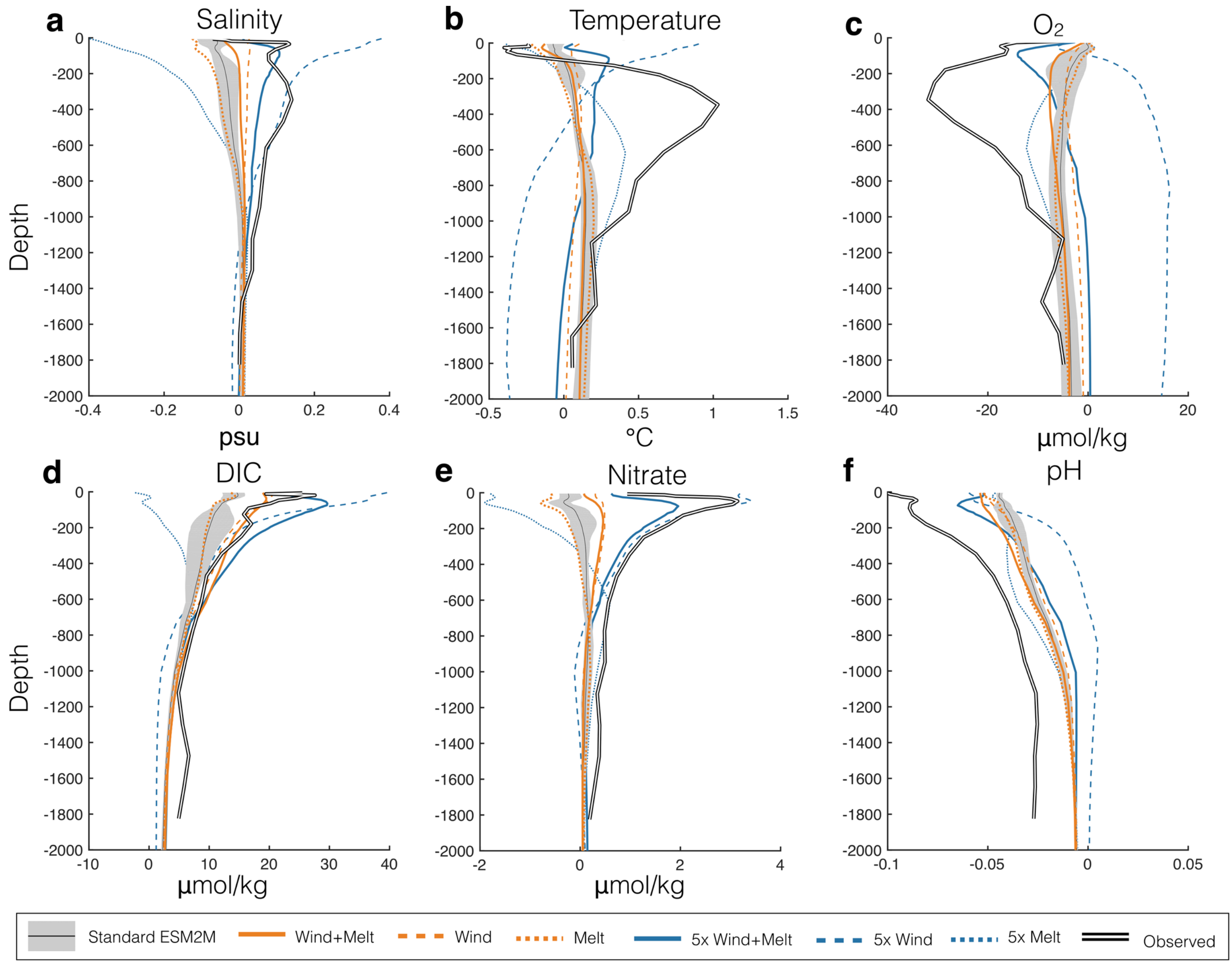

Extended Data Fig. 7 | Vertical profile of anomalies. Change in **a**, salinity, **b**, temperature, **c**, oxygen, **d**, dissolved inorganic carbon (DIC), **e**, nitrate and **f**, pH between the periods 2014-2019 and 1985- 2005 averaged over the area South of 60°S. The double black line shows the observed anomaly, the thin black line shows the 5-ensemble-member mean standard ESM2M simulation, the dotted blue line shows the ESM2M with only meltwater added, the dashed blue line shows the ESM2M with only winds increased and the solid blue line shows the melt+wind simulation. The orange lines shows the same as blue lines, but with the milder perturbation scenarios (0.2x wind and melt). The black shaded region shows the 90% uncertainty range due to natural variability from the ESM2M 5-member ensemble. The same shading applies to all profiles shown, but has been omitted for clarity of presentation.

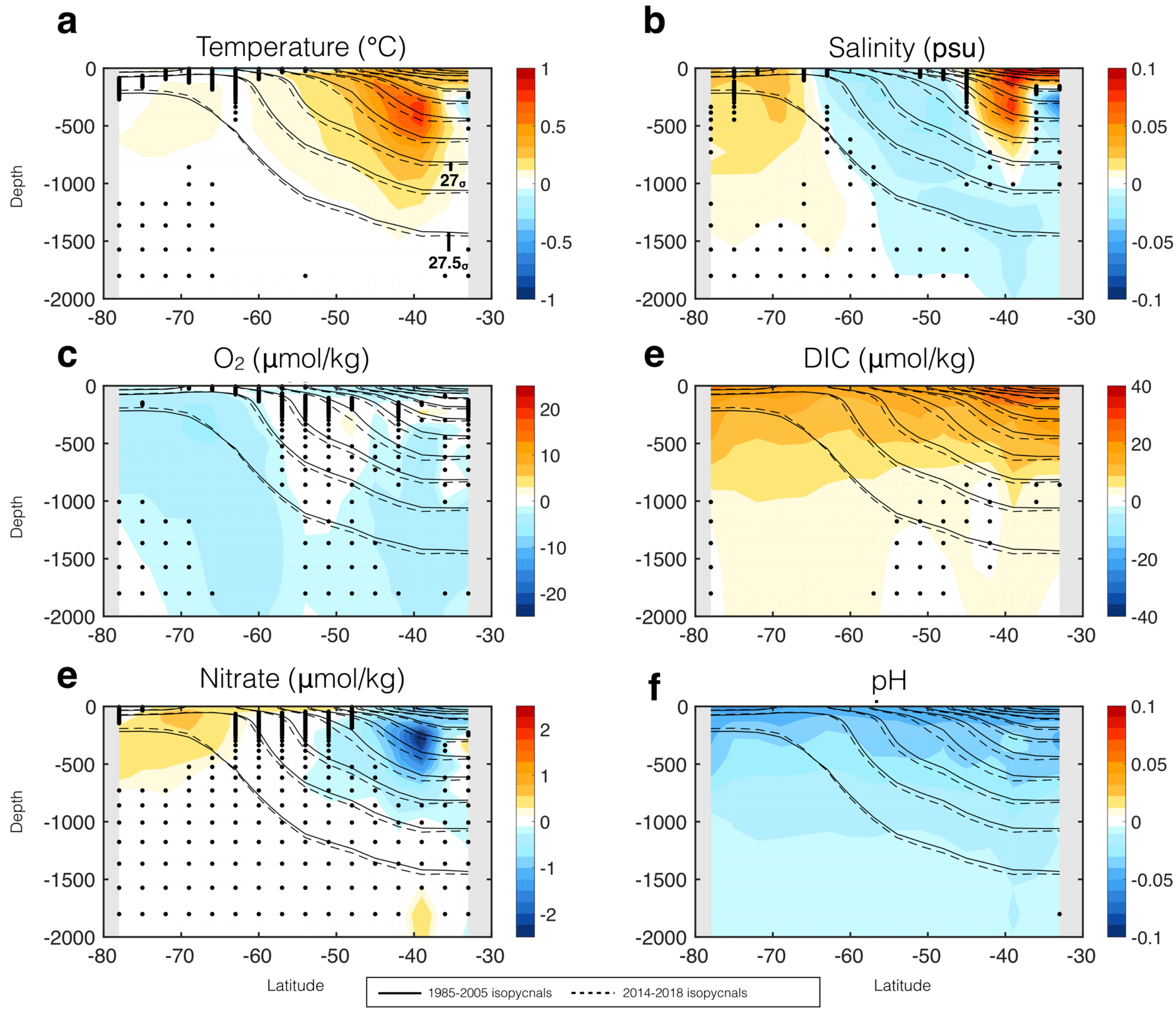

Extended Data Fig. 8 | Wind-only scenario simulated decadal changes. 5-member ensemble mean of the zonal mean differences in **a**, temperature, **b**, salinity, **c**, oxygen, **d**, dissolved inorganic carbon (DIC), **e**, nitrate and **f**, pH between years 2014-2019 of the wind-only RCP8.5 ESM2M simulation and years 1985–2005 of the standard simulation. Solid and dashed lines show zonal mean 1985- 2005 and 2014–2019 isopycnal surfaces respectively. The stippling indicates where the differences are not significant at the 90% level (see Methods). Here, the model is not sub-sampled to show the whole Southern Ocean response to the wind perturbation.

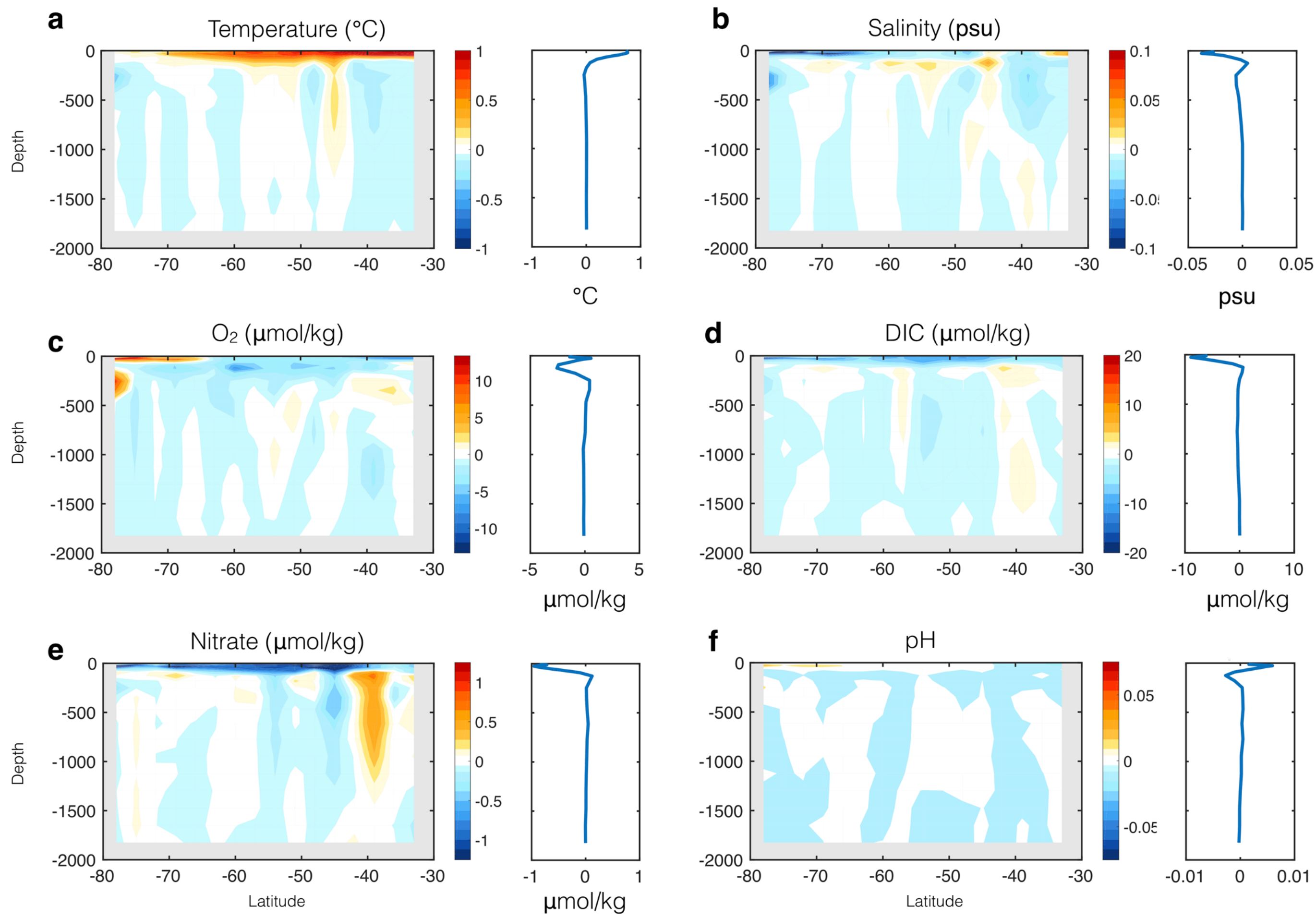

Extended Data Fig. 9 | Seasonal bias correction. Difference between the December-May and annual means for **a**, temperature, **b**, salinity, **c**, oxygen, **d**, DIC, **e**, nitrate, and **f**, pH in the SOCCOM dataset. The colored depth-latitude panels show the zonal mean difference, and the depth profile to the right of each colored panel show the corresponding zonal and meridional mean.

	Standard	Wind+Melt	5×Wind+Melt
Temperature	0.11±0.01	**0.16**±0.01	0.15±0.01
Salinity	0.03±0.02	0.27±0.02	**0.33**±0.03
Oxygen	0.20±0.08	**0.50**±0.05	0.43±0.02
DIC	0.62±0.01	**0.70**±0.01	0.63±0.01
Nitrate	-0.03±0.02	0.20±0.03	**0.25**±0.01
pH	0.72±0.01	**0.81**±0.01	0.76±0.01

Extended Data Fig. 10 | Table ED10. Spatial correlations of the ESM2M standard historical-RCP8.5 (Fig. 3), WM (Fig. 5), and 5×WM (supplementary Fig. ED5) ensemble scenario anomalies with the observed anomalies, as well as the 90% uncertainty in the mean based on 5 ensemble members. The bold text indicates the largest correlation for each field.